Efficient Organic Iodide and Iodine vapour phase capture by Viologen-based organic framework

A Thesis

submitted to

Indian Institute of Science Education and Research, Pune in partial fulfilment of the requirements for the MSc. Degree Programme

by

Yashasvi Banyla

(20226207)

Under the guidance of

Prof. Sujit K. Ghosh

Indian Institute of Science Education and Research, Pune

Dr. Homi Bhabha Road,

Pashan, Pune 411008, INDIA.

April, 2024

Supervisor: Prof. Sujit K. Ghosh

Student: Yashasvi Banyla

Certificate

This is to certify that this thesis entitled *Efficient Organic Iodide and Iodine Vapor Phase Capture by Viologen-based organic framework*, towards the partial fulfilment of the MSc. degree program at the Indian Institute of Science Education and Research, Pune represents research work carried out by **Yashasvi Banyla** (20226207) at the Indian Institute of Science Education and Research under the supervision of **Prof. Sujit K. Ghosh**, Department of Chemistry, during the academic year 2023- 2024.

Prof. Sujit K. Ghosh
Research Supervisor
E-Mail: sghosh@iiserpune.ac.in
Contact No.: +91(20)25908076

Committee:

Prof. Sujit K. Ghosh
Dr. Shabana Khan

This thesis is dedicated to my parents

Declaration

I hereby declare that the matter embodied in the report entitled *Efficient Organic Iodide and Iodine Vapour Phase Capture by Viologen-based Organic Framework*, are the results of the work carried out by me at the Department of Chemistry, Indian Institute of Science Education and Research, Pune, under the supervision of Prof. Sujit K. Ghosh and the same has not been submitted elsewhere for any other degree.

Yashasvi Banyla

Reg. No.: 20226207

Date: 09-04-2024

Table of Contents

Abstract……8
Acknowledgement……...9
1. Chapter 1 Introduction…….....10
1.1 Porous Materials…….…10
1.2 Nuclear Energy Generation: Challenges and Concerns…….…….....11
1.3 Potential of Porous Sorbents: Capturing ROI…….....12
1.4 Designing Cationic Covalent Organic Polymer for ROI Sequestration…….…..13

2. Chapter 2 Material and Methods……...…….15
2.1 Materials…….…..…15
2.2 General Characterization and Physical Measurements……...…….....15
2.3 Synthesis…….….16

3. Chapter 3 Results and Discussion……..…23
3.1 Characterization……...23
3.2 ROI Sorption Studies……...27
3.3 Post-Capture Characterization…….31
3.4 Recovery and Recyclability…….35

4. Chapter 4 Conclusion…….…….36

5. Appendix…….37

6. Reference……...…….52

List of Tables

Table 5.1 Fitting data of Methyl Iodide and iodine-loaded IP-VOFs……....40

Table 5.2 Elemental Analysis Data of IP-VOF 1 to 3……...……...41

List of Figures

Figure 1.1 Schematic Representation……..…14

Figure 2.1 Synthesis scheme of 1,1'-bis-(2,4-dinitrophenyl)-[4,4'-bipyridine]-1,1'-diium dichloride……....17

Figure 2.2 Structure of 1,3,5-tris(4-aminophenyl)-benzene…….....17

Figure 2.3 Synthesis scheme of 4,4',4"-(pyridine-2,4,6-triyl)-trianiline……...….18

Figure 2.4 Synthesis scheme of 4,4',4"-(1,3,5-triazine-2,4,6-triyl)-trianiline……...….19

Figure 2.5 Synthesis scheme of IP-VOF 1…….20

Figure 2.6 Synthesis scheme of IP-VOF 2…….21

Figure 2.7 Synthesis scheme of IP-VOF 3…….21

Figure 2.8 Generalized synthesis scheme for IP-VOFs…….....22

Figure 3.1 General Characterization……..25

Figure 3.2 TEM Images of IP-VOF…….26

Figure 3.3 Elemental Mapping from TEM of IP-VOFs……...27

Figure 3.4 and 3.5 Capture Studies…….30

Figure 3.6 and 3.7 Post Capture Characterization……..…32

Figure 3.8 and 3.9 Elemental Mapping from TEM of CH_3I@IP-VOFs and I_2@IP-VOFs ……34

Figure 5.1 and 5.2 Schematic Diagram of Static Setup……....37

Figure 5.3 Schematic Diagram of Dynamic Setup……....38

Figure 5.4 and 5.5 Digital Image of Experimental Setup……39

Figure 5.6 Thermogravimetric Analysis (TGA) of IP-VOFs……41

Figure 5.8 Zeta-Potential Measurement of IP-VOFs, CH_3I@IP-VOFs and I_2@IP-VOFs.....42

Figure 5.9 Powder X-Ray Diffraction (PXRD) OF IP-VOFs.....43

Figure 5.10 and 5.11 N_2 (77 K) and CO_2 (195 K) Adsorption-Desorption Isotherm.....43

Figure 5.12 Energy-dispersive X-ray spectroscopy (EDS) of IP-VOFs.....44

Figure 5.13 Fitting of CH_3I and I_2 Capture Kinetics.....45

Figure 5.14 HR-TEM Images of CH_3I@IP-VOFs and I_2@IP-VOFs.....46

Figure 5.15 Energy-dispersive X-ray spectroscopy (EDS) of CH_3I@IP-VOFs.....47

Figure 5.16 Energy-dispersive X-ray spectroscopy (EDS) of I_2@IP-VOFs.....48

Figure 5.17 Thermogravimetric Analysis (TGA) of CH_3I@IP-VOFs and I_2@IP-VOFs.....49

Figure 5.18 Retention Efficiency of CH_3I@IP-VOFs.....50

Figure 5.19 Retention Efficiency of I_2@IP-VOFs.....51

Figure 5.20 Schematic Diagram of Iodine Recovery Setup.....52

Figure 5.21 Digital Image of Recovered Iodine Crystals.....52

Abstract

Sequestration of radioactive organic iodide (ROIs) during fuel reprocessing in nuclear power plants is significant to ensure nuclear safety, protect the environment, and safeguard public health. Radioactive molecular Iodine (I_2) and organic iodides, mainly Methyl Iodide (CH_3I), coexist at low concentrations in the off-gas stream of nuclear power plants. Despite several materials being reported for the adsorption of ROIs, developing an effective adsorbent with high adsorption and retention efficiency, recyclability, and recovery is still a significant challenge. In this study, we aimed to understand the role of framework-integrated functionalities in organic iodide sequestration. We achieved this by varying the number of N-heteroatomic sites in a series of chemically stable porous covalent organic polymers (COPs). The study discovered that the I_2 adsorption capacity in COPs is positively linked to the presence of N-heteroatomic or heterocyclic functionalities such as bipyridyl, pyridine, and triazine sites. The highest capacity of 5.53 $g.g^{-1}$ was recorded at 348 K for triazine-based COP. On the other hand, the CH_3I adsorption capacity showed a unique trend, with pyridine-based COPs exhibiting the highest adsorption efficiency of 4.92 $g.g^{-1}$ and 3.47 $g.g^{-1}$ at 423 K and 348 K, respectively, surpassing most of the adsorbents reported for methyl iodide capture. This work contributes to a deeper insight into I_2/CH_3I adsorption mechanisms.

Acknowledgement

I would like to express my heartfelt gratitude to my research supervisor, Prof. Sujit K. Ghosh, for granting me the opportunity to work in his lab and providing me with an excellent research environment. Working under his supervision has been an immense privilege, and his valuable guidance and discussions supported me in completing my thesis project and will continue to guide me in the future. I would also like to sincerely acknowledge the current director of the Indian Institute of Science Education and Research (IISER), Pune, Prof. Sunil S. Bhagwat, for creating a world-class research facility and fostering a vibrant research environment. I am extremely thankful to my thesis advisory committee (TAC) members, Dr. Shabana Khan (IISER, Pune), for their valuable suggestions and advice. I am grateful to all the IISER Pune faculty members for teaching me and instilling in me the research culture. I would like to express my appreciation to all my labmates from the SKG group, and I would like to extend a special thanks to Dipanjan Majumder, my mentor, for his diligent efforts, trust in me, and most importantly, for being an exceptional mentor. Lastly, I want to thank my beloved family, my partner Aditya, and all my dear friends for providing me with emotional support and being there for me during the most challenging times.

1. Introduction

1.1 Porous Materials

A brief discussion on porous materials is included in this section. Porous materials are the class of materials having pores, cavities, channels, or interstices. The properties of a porous material may vary depending on the size, shape, and arrangement of the pores, as well as the porosity (the ratio of the total pore volume relative to the apparent volume of the material) and constituents of the material itself. Porous solids possess significant scientific and technological value, owing to their capability to interact with atoms, ions, and molecules both at their surface and within the material. These materials have long been utilized for ion exchange, separation through adsorption, and catalysis. The ordered structure of solids like zeolites is particularly beneficial for numerous applications. Porous materials possess tiny voids or openings known as pores, which are categorized by their size. Micropores refer to pores smaller than 2 nm, mesopores range between 2 nm and 50 nm, and macropores exceed 50 nm in size. The effectiveness of porous materials in fulfilling their intended purpose in a specific application is determined by the size, shape, and capacity of these void spaces. [1]

Recently, Advanced Porous Materials (APMs) have emerged as a novel class of porous materials, offering the ability to customize them to suit specific application needs. The intricate interplay of organic and inorganic materials creates a vast range of structural possibilities, thus making APMs a remarkable stride forward in material science and chemistry. Advanced Porous Materials consist of various types of materials such as Metal-Organic Framework (MOF), Covalent Organic Framework (COF), Porous Organic Polymer (POP), Metal-Organic Polyhedra (MOP), Metal-Organic Gel (MOG), etc. They are superior to other porous materials due to their synthetically simple approaches. These unique properties are not found in traditional porous materials. APMs have the potential to revolutionize various domains related to energy and the environment, thereby creating new possibilities for advancement.

1.2 Nuclear Energy Generation: Challenges and Concerns

Nuclear power plants are one of the alternative sources of renewable energy. Nuclear energy is clean and economically competitive without causing greenhouse gas emissions. Although it is facing major issues related to operational safety and safe disposal of generated radioactive waste, it remains an important part of today's energy mix. One of the major problems in nuclear plants, during the generation of nuclear energy, the used nuclear fuel rods need to be dissolved into concentrated hot nitric acid for reprocessing. During this dissolution method, apart from the molecular iodine, nitric acid vapour, NO_2, and N_2O_5, another highly radioactive dissolved off-gas (DOG) species - organic iodides e.g., methyl iodide (CH_3I) and ethyl iodide (CH_3CH_2I) are generated. Radioactive organic iodide (ROI) vapour is extremely toxic to living beings due to its substantially higher activity [3]. It therefore has drawn a significant attention of people, especially in the event of a nuclear disaster. Therefore, considering both the aspects of the environment as well as human health along with futuristic development and secure generation of nuclear energy, efficient sequestration of these radioactive volatile gases from the air has received a topical research interest in recent years. However, it was found that trapping these ROI species is challenging owing to their lower adsorption rate and thus further exhibit poor retention efficiency. The main components of such gaseous waste streams include the fission products technetium (^{99}Tc), caesium (^{137}Cs), and strontium (^{90}Sr), as well as actinides, lanthanides and various volatile radionuclides (^{129}I, ^{131}I, ^{3}H, ^{14}C, ^{85}Kr, etc.). Particular attention should be paid to particularly abundant iodine compounds, as radioactive iodine will likely form organic compounds such as methyl iodide and ethyl iodide with hydrocarbons and other volatile organic compounds. ^{129}I is a highly volatile long-lived isotope with a half-life ($t_{1/2}$) of ~1.57×10^7 years, which needs to be captured and reliably stored during its long decay. In contrast, ^{131}I is a volatile short-lived isotope with a $t_{1/2}$ of ~8.02 days, which needs to be captured immediately after being released, as it tends to accumulate and become concentrated in the thyroid gland, which can severely harm the thyroid gland and a significant impact on human metabolism. This can cause a range of symptoms, including dizziness, slurred speech, visual disturbances, irritability, loss of muscle control, drowsiness, delirium, serious mental disorders, coma, and even death so it is essential to remove ROIs before discharging the off-gas.

1.3 Potential of Porous sorbents: capturing ROI

Recent research has identified different types of porous sorbents that have demonstrated significant potential in capturing radioactive iodine and its compounds. When compared to traditional liquid scrubbing methods, adsorption-based processes have the advantage of being simpler to operate, requiring less maintenance, and avoiding the use of highly corrosive solutions. Therefore, scientists are currently focusing their efforts on developing adsorbents that can effectively capture iodine. This includes a variety of materials such as silver, silver-impregnated silica, alumina, silver-functionalized aerogels, titano-silicates, mesoporous silica, macro reticular ion exchange resins [4], metal-organic frameworks (MOFs), covalent-organic frameworks (COFs), porous organic polymers (POPs), covalent organic polymers (COPs), and conjugated polymers. Among these materials, porous sorbents such as COPs, POPs, COFs, and MOFs show the most potential for capturing radioactive iodine due to their high removal efficiency and adsorption capacities. Additionally, these materials boast high thermal stability, fast kinetics, low maintenance costs, and a wide range of structures and functionalisation options. [2]

Several ways can be used to enhance the adsorption of iodine species. In the case of I_2, effective strategies are used which include, integrating electron-rich heteroatoms like oxygen (O), sulphur (S), and nitrogen (N), or π-donors such as benzene rings, double/triple bonds, and other aromatic compounds, into adsorbents to create charge-transfer complexes that bind electron-deficient I_2, and modifying the adsorbent with ionic groups, to attract I_2 using Coulombic interaction or utilising adsorbents that contain Ag to generate silver iodide (AgI) precipitation. Incorporating cationic groups with free anions inside the adsorbent could enhance the adsorption of I_2 vapour by creating strong electrostatic interactions with polyiodide species formed in situ. The counter anions integrated into the framework facilitate energetically favourable interactions with iodine in the vapour phase [5,6]. Compared to I_2, capturing CH_3I is more challenging due to weaker intermolecular forces. Currently, CH_3I capture is primarily achieved by catalytic decomposition on adsorbents containing silver (Ag) to form AgI, or through an N-methylation reaction on nucleophilic nitrogen (N) sites to form pyridinium or quaternary ammonium salts. The high adsorption capacity of iodine is also governed by textural features such as surface area, pore size, and pore volume of the porous sorbents. Based on these insights, it is speculated that adsorbents containing abundant Ag sites or nucleophilic N sites with rich surface area can exhibit high capture

capacity for both I_2 and CH_3I. However, given the high cost and poor recyclability of Ag-based adsorbents, developing porous N-rich adsorbents is a better choice for simultaneously capturing I_2 and CH_3I [7,8].

Aiming at selective removal of both elemental iodine and methyl iodide under practical conditions, and given that radioactive molecular iodine and organic iodides are present together in off-gas streams, it's essential to develop efficient adsorbents capable of capturing both species. It is widely recognized that fuel rods have been frequently subjected to HNO_3 treatment at elevated temperatures (up to 150 °C). As a result, the CH_3I containing off-gas is accompanied by H_2O, HNO_3, NO_2, and N_2O_5, thus rendering the material's viability under these extremely harsh conditions a major challenge. The adsorption performance of the material is significantly impacted by high humidity levels, thus calling for a material that can endure such conditions [13,14].

1.4 Designing Cationic Covalent Organic Polymer for ROI Sequestration

Taking all these factors into consideration, herein, in this work, we designed and synthesised three robust 'cationic' covalent organic polymers (COPs), namely IP-VOF 1, IP-VOF 2, and IP-VOF 3, where 'IP' stands for IISER Pune, and 'VOF' stands for 'Viologen Organic Framework'. The framework of IP-VOF was constructed through nucleophilic bipyridyl linkages, the densely functionalised bipyridine building blocks, and Heteroatomic N sites, which are expected to interact with the elemental iodine molecule through the electron-pair effect with enhanced binding affinity and to act as the substrate of the methylation reaction for the immobilization of methyl iodide [12]. To the best of our knowledge, this is the first time that "cationic polymer" is used for both I_2 and CH_3I adsorption. We deliberately chose a series of three VOFs, constructed from the covalent threading of 1,1'-bis-(2,4-dinitrophenyl)-[4,4'-bipyridine]-1,1'-diium dichloride (Viologen Precursor) (VIO) with three different triamines. The architecture of the structurally analogous VOFs featuring various N-containing heterocyclic structural moieties including benzene core tri-phenyl triamine (for IP-VOF 1), pyridine core tri-phenyl triamine (for IP-VOF 2), and triazine core tri-phenyl triamine (for IP-VOF 3) as a specific recognition site which can serve as variable interactions with ROIs. The programmed functional moieties, or chemical groups, present in the VOF play a crucial role in dictating the interactions between the surface of the VOFs and the ROI species, thereby significantly altering the affinity between them. This, in turn, offers a deeper

understanding of the role of various nitrogen-containing sites in the sorption process of ROIs, which can help in designing more efficient and effective sorbent materials for various practical applications. The investigation revealed I_2 uptake capacities were found to correspond positively with the adsorbent's nitrogen content, as a systematic increase in Iodine uptake capacities was observed when moving from IP-VOF 1 to IP-VOF 3 under static and dynamic conditions. Among all, IP-VOF 3 displayed the most noteworthy capacity for I_2 uptake in both dry and humid environments at 75 °C, as well as at an elevated temperature of 150 °C. However, in the case of Methyl Iodide (CH_3I) adsorption, IP-VOF 2 surpassed all the benchmark adsorbents with its ultrahigh adsorption efficiency at 150 °C (fuel rod reprocessing temp.) as well as at 75 °C. Additionally, it has been discovered that these highly stable and effective adsorbents are capable of cyclically adsorbing ROIs with minimal impact on their sorption. This approach may lead to the emergence of a multitude of potent adsorbents with an exceptionally high enrichment index for radioactive ROI species found in nuclear waste.

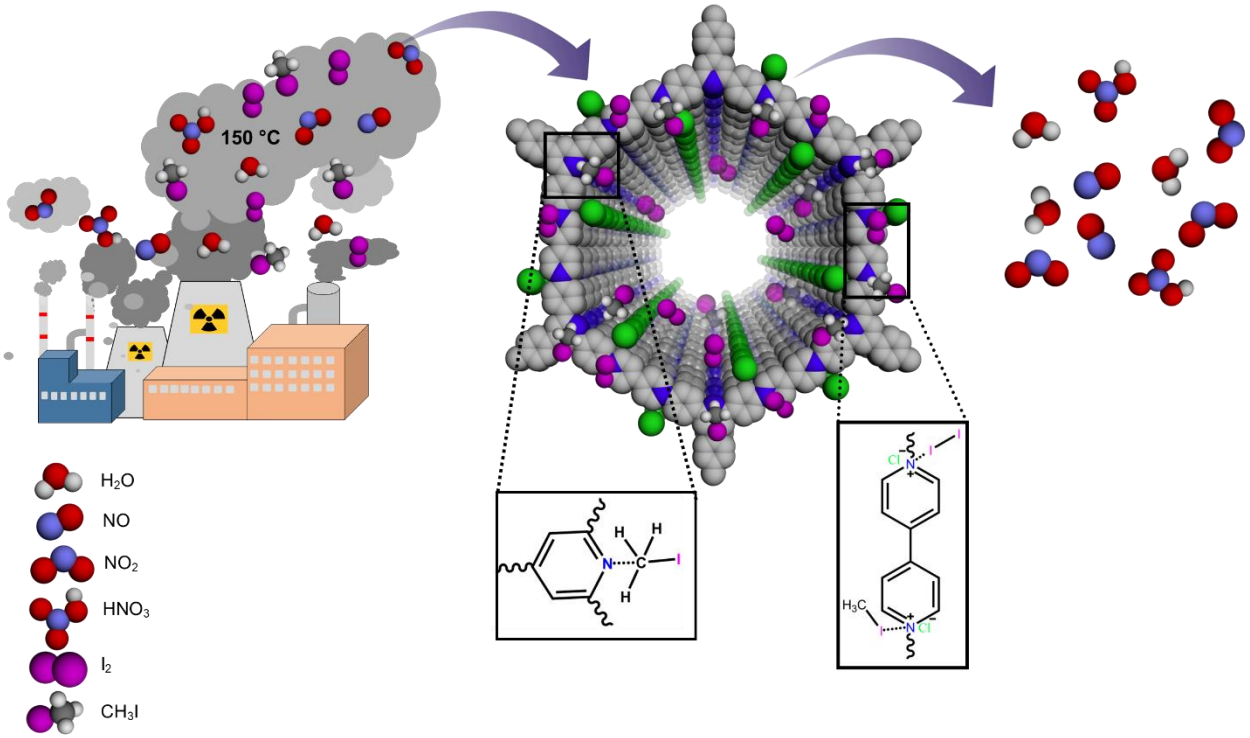

Figure 1.1: Schematic Representation of Selective Capture of Hazardous ROI waste by IP-VOF.

2. Materials and Methods

2.1 Materials

All the reagents, starting materials and solvents were commercially purchased from Sigma-Aldrich, TCI Chemicals, Spectrochem, and Rankem depending on their availability and used without further purification.

2.2 General Characterizations and Physical Measurements:

2.2.1 Fourier transform infrared spectroscopy (FT-IR): The FT-IR spectra were acquired using NICOLET 6700 FT-IR spectrophotometer using KBr pellet in 500-4000 cm-1 range.

2.2.2 Thermogravimetric analysis (TGA): Thermogravimetric analyses were recorded on a Perkin Elmer STA 6000 TGA analyser by heating the samples from 30°C to 800 °C under N_2 atmosphere with a heating rate of 10 °C min^{-1}.

2.2.3 Powder X-ray diffraction (PXRD): Powder X-ray diffraction (PXRD) experiments were performed on a Bruker D8 Advanced X-ray diffractometer at room temperature using Cu Kα radiation (λ = 1.5406 Å) at a scan speed of 0.5 °min^{-1} and a step size of 0.01° in 2θ**.**

2.2.4 Transmission electron microscopy (TEM): TEM and high-resolution TEM imaging were performed on the HRTEM (JEM-2200FS, JEOL) operating at an acceleration voltage of 200 kV. For TEM analysis, all the samples were dispersed in ethanol (0.5 mg/mL) and sonicated for 20 minutes. Then, the samples were left for 5 min, and the upper part of the solution was taken for preparing TEM samples on a lacey carbon-coated copper grid (Electron Microscopy Science, 200 mesh).

2.2.5 Solid-state nuclear magnetic resonance (NMR) spectroscopy: Solid-state ^{13}C cross polarization-magic angle spinning (CP-MAS) spectra were conducted on a Bruker 500 MHz NMR spectrometer with a CP-MAS probe. Carbon chemical shifts are expressed in parts per million (δ scale).

2.2.6 High-resolution mass spectroscopy (HRMS): The mass analysis of the starting material was carried out using high-resolution mass spectrometry (HRMS-ESI-Q-TOF LC-MS) and Applied Biosystem 4800 PLUS matrix-assisted laser desorption/ionisation (MALDI) TOF/TOF analyser.

2.2.7 Nitrogen adsorption-desorption isotherm measurements: N_2 gas adsorption-desorption measurements were performed using the BelSorp-Max instrument (Bel Japan). Before adsorption measurements, the activated samples were heated at 120 °C under vacuum for 12 hours using BelPrepvacII.

2.2.8 X-ray photoelectron spectroscopy (XPS): As-obtained powder samples were stuck to conductive paste and then measured by X-ray photoelectron spectroscopy using K-Alpha+model (Thermo Fischer Scientific, UK) with Al Kα source.

2.2.9 Zeta potential: Zeta potential measurements were performed on Anton Paar Litesizer 500 series instrument. Measurement cell: Omega cuvette Mat. No. 155765, Target temperature 25.0 °C, Equilibration time – (Series parameter), Henry factor 1.1 (Other), Adjusted voltage (Automatic Mode), Number of runs 20, Solvent – water.

2.2.10 Raman measurements: Raman spectra were acquired with an Xplora PLUS Raman microscope (Horiba Company) (633 nm laser and a 1200 lines/mm grating).

2.3 Synthesis

Synthesis of cationic organic frameworks for ROI capture has rarely been explored. In the literature, very few reports are present on the direct synthesis of ionic organic frameworks, and viologen-based organic frameworks are one of them, which have been synthesized via Zincke's

reaction, which is an effective tool to synthesize viologen-based compounds in a single-step, but this reaction has not been used much to synthesize extended porous organic networks. In our quest to develop highly stable π-conjugated covalent materials, we have explored the use of the Zincke reaction between 1,1′-bis(2,4-dinitrophenyl)- [4,4′-bipyridine]-1,1′-diium dichloride (VIO) and an aromatic amine. To expedite the reaction, we employed microwave (MW) heating modes.

2.3.1 Synthesis of 1,1'-bis-(2,4-dinitrophenyl)-[4,4'-bipyridine]-1,1'-diium dichloride (Viologen Precursor) **(VIO)**: The synthesis follows a known procedure with a slight modification, 25.6 mmol of 4,4‘-bipyridine and 89.6 mmol of 2,4-dinitro-chlorobenzene in CH_3CN (150 ml) was stirred at 90°C for 3 days under reflux. The resulting solution was a clear brown colour. The mixture was filtered and washed with MeCN and diethyl ether. After drying in vacuo, 1,1’-Bis-(2,4-dinitrophenyl)-4,4’-bipyridinium dichloride was obtained [9,10].

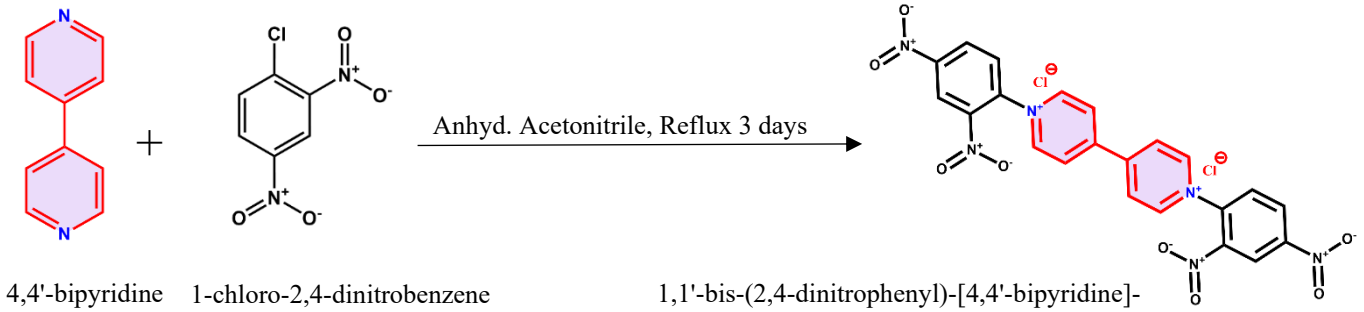

4,4'-bipyridine 1-chloro-2,4-dinitrobenzene 1,1'-bis-(2,4-dinitrophenyl)-[4,4'-bipyridine]-1,1'-diium dichloride

Figure 2.1: Synthesis scheme of 1,1'-bis-(2,4-dinitrophenyl)-[4,4'-bipyridine]-1,1'-diium dichloride

2.3.2 1,3,5-tris(4-aminophenyl)-benzene **(BZA)**

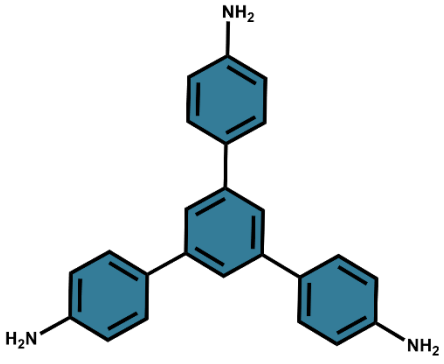

Figure 2.2: Structure of 1,3,5-tris(4-aminophenyl)-benzene.

2.3.3 Synthesis of 4,4',4''-(Pyridine-2,4,6-triyl)-trianiline **(PYA)**: 4,4',4''-(pyridine-2,4,6-triyl)-trianiline was synthesized using a previously reported method. Firstly, 2,4,6-tris(4-nitrophenyl)-pyridine was synthesised. To do this, 10 mmol of 4-nitrobenzaldehyde and 20 mmol of 4-nitro acetophenone were dissolved in 25 ml of acetic acid. Then, 10 g of ammonium acetate was added to the mixture and heated at 110°C for 3 hours. A dark red precipitate was filtered and washed with acetic acid and cold ethanol. After drying the precipitate at around 80°C, it was found to be 2,4,6-tris(4-nitrophenyl)-pyridine, which was further used in the next step for amine preparation. In the next step, 1.5 g of the 2,4,6-tris(4-nitrophenyl)-pyridine was dissolved in 20 ml of ethanol and 60 mg of $FeCl_3.6H_2O$ and 200 mg of activated carbon were added to this solution, and it was heated under reflux conditions for 30 minutes. Then, 4 mL of hydrazine hydrate in 4 mL of ethanol was added dropwise to the mixture and refluxed for 12 hours. After that, the mixture was filtered while hot, and the filtrate was poured into excess distilled water. A high yield of yellow precipitate was obtained, which was filtered, washed with water, and dried at 60°C overnight.

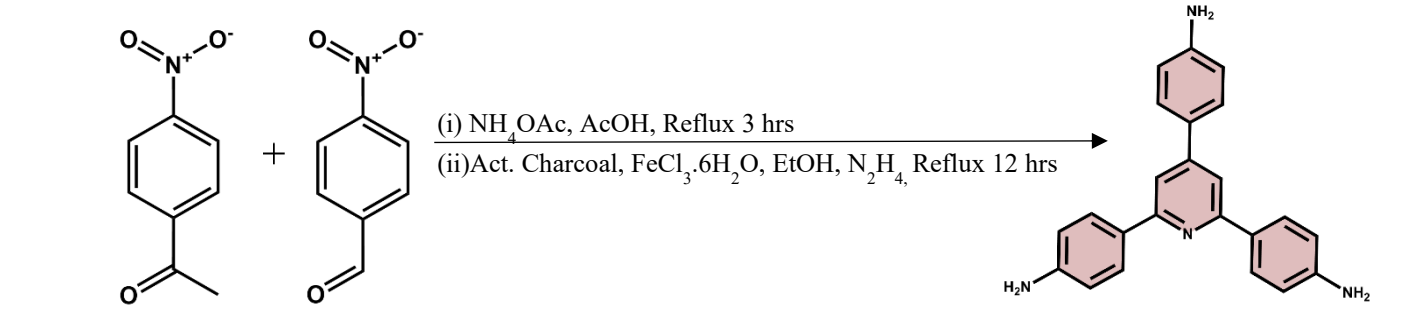

Figure 2.3: Synthesis scheme of 4,4',4''-(pyridine-2,4,6-triyl)-trianiline

2.3.4 Synthesis of 4,4',4''-(1,3,5-triazine-2,4,6-triyl)-trianiline **(TTA)**: TAPT was synthesized via superacid catalysed trimerization of 4-aminobenzonitrile. In a typical synthesis, 6.538 mmol 4-aminobenzonitrile was taken in a round bottom flask at 0 ºC. Then 2 mL (22.2 mmol) trifluoromethanesulfonic acid was added dropwise for 20 min maintaining the temperature at 0 ºC. The resultant mixture was stirred for 24 hours at room temperature in an inert atmosphere. After that, 20 mL of distilled water was added to the mixture and neutralized by adding 2M NaOH solution until the pH reached 7. Initially, with an increase in pH, the orange precipitate dissolves to give a bright orange solution, which upon a further increase in pH gives a pale-yellow precipitate. The resultant pale-yellow product was filtered and washed several times with distilled water [10,11].

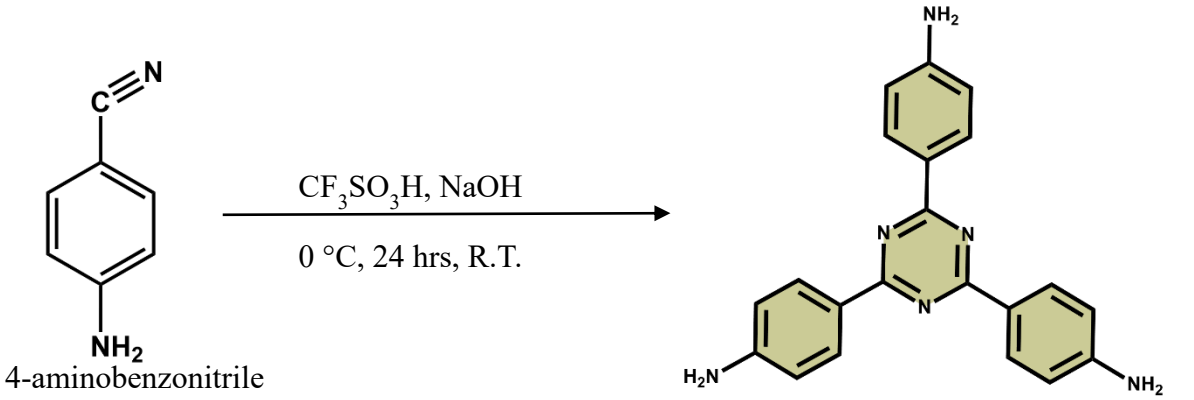

4-aminobenzonitrile

4,4',4''-(1,3,5-triazine-2,4,6-triyl)-trianiline

Figure 2.4: Synthesis scheme of 4,4',4''-(1,3,5-triazine-2,4,6-triyl)-trianiline.

- IP-VOF 1,2, and 3 were synthesised from 1,1'-bis-(2,4-dinitrophenyl)-[4,4'-bipyridine]-1,1'-diium dichloride (VIO) and 1,3,5-tris(4-aminophenyl)-benzene (BZA)/4,4',4''-(Pyridine-2,4,6-triyl)-trianiline (PYA) / 4,4',4''-(1,3,5-triazine-2,4,6-triyl)-trianiline **(**TTA) respectively, and was found to be insoluble in various solvents, which indicated the formation of an extended network. Furthermore, to remove occluded solvent molecules, VOF was solvent exchanged in ethanol for 4-5 days and then desolvated under vacuum at 100°C.

2.3.5 Synthesis of IP-VOF 1: It was synthesised from precursors VIO and BZA via Zincke's reaction. A 4:1 mixture of ethanol and water was used to mix 0.5 mmol of BZA and 0.5 mmol of VIO, which was heated at 100°C for 2 hours under microwave irradiation. The addition of water helped prevent the degradation of the Zincke salt. The mixture was filtered, washed with water and ethanol/methanol, and dried under a vacuum.

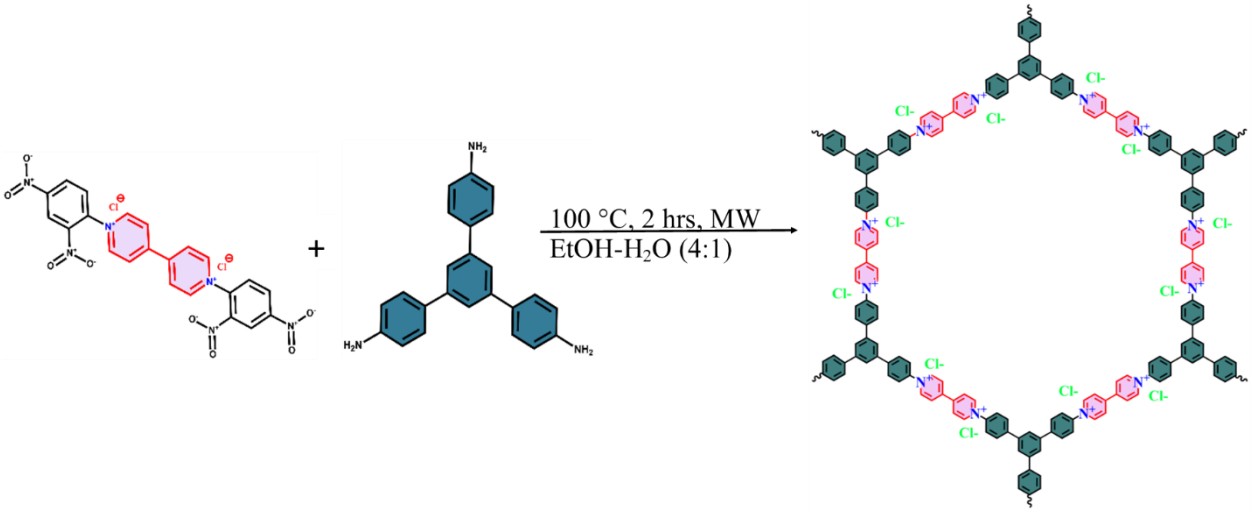

Figure 2.5: Synthesis scheme of IP-VOF 1.

2.3.6 Synthesis of IP-VOF 2: IP-VOF 2 was synthesized using the same procedure as IP-VOF 1 but with PYA precursor (0.5 mmol).

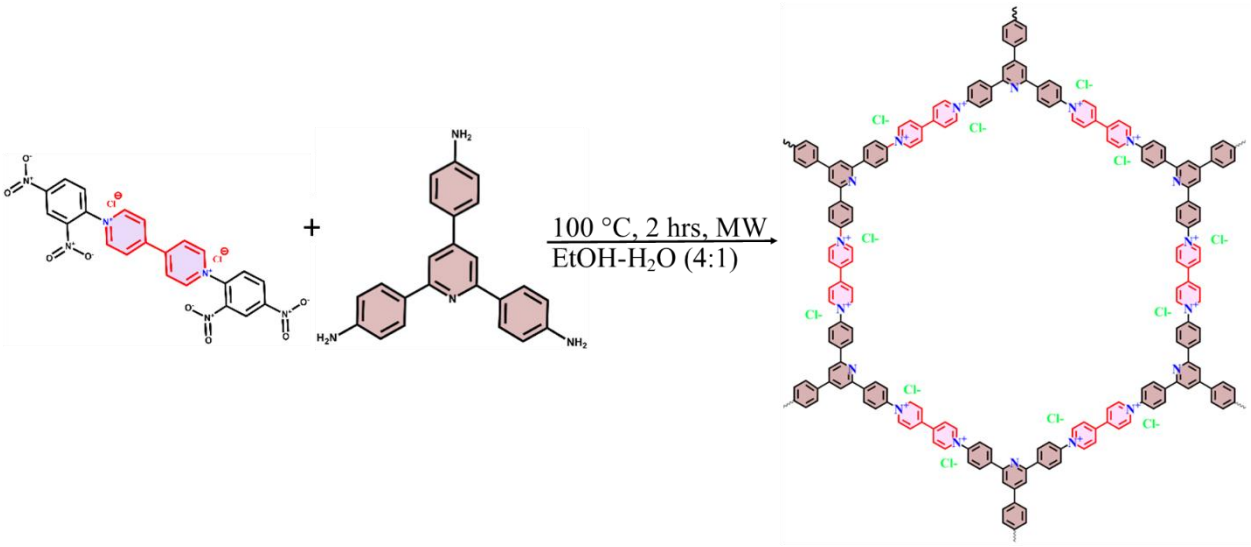

Figure 2.6: Synthesis scheme of IP-VOF 2.

2.3.7 Synthesis of IP-VOF 3: IP-VOF 3 was synthesized using the same procedure as IP-VOF 1 but with TTA precursor (0.5 mmol).

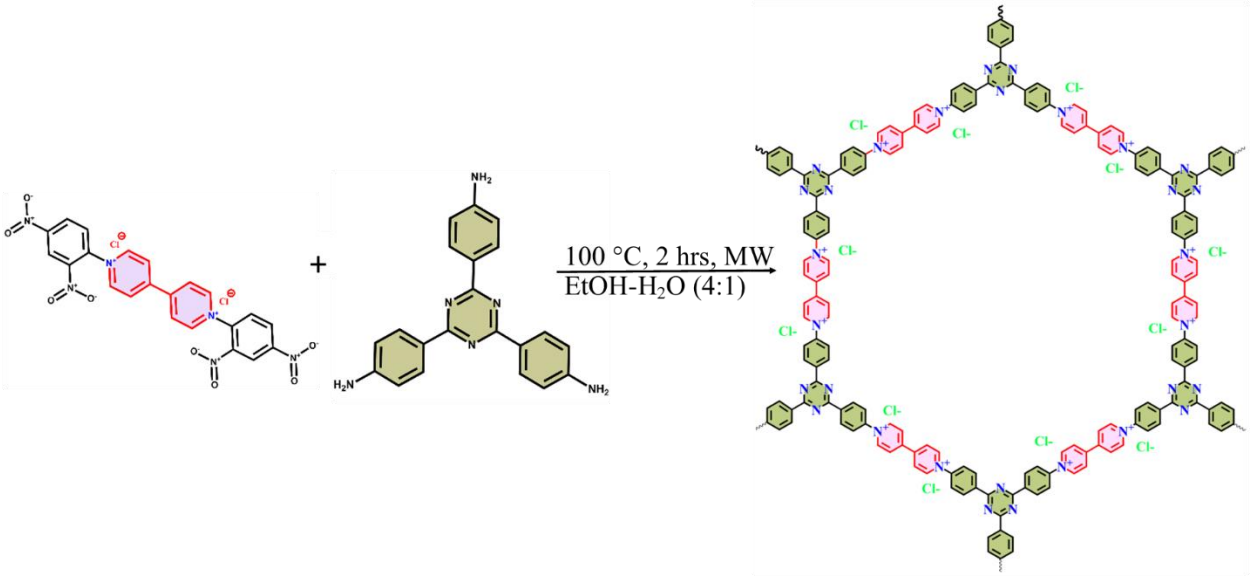

Figure 2.7: Synthesis scheme of IP-VOF 3.

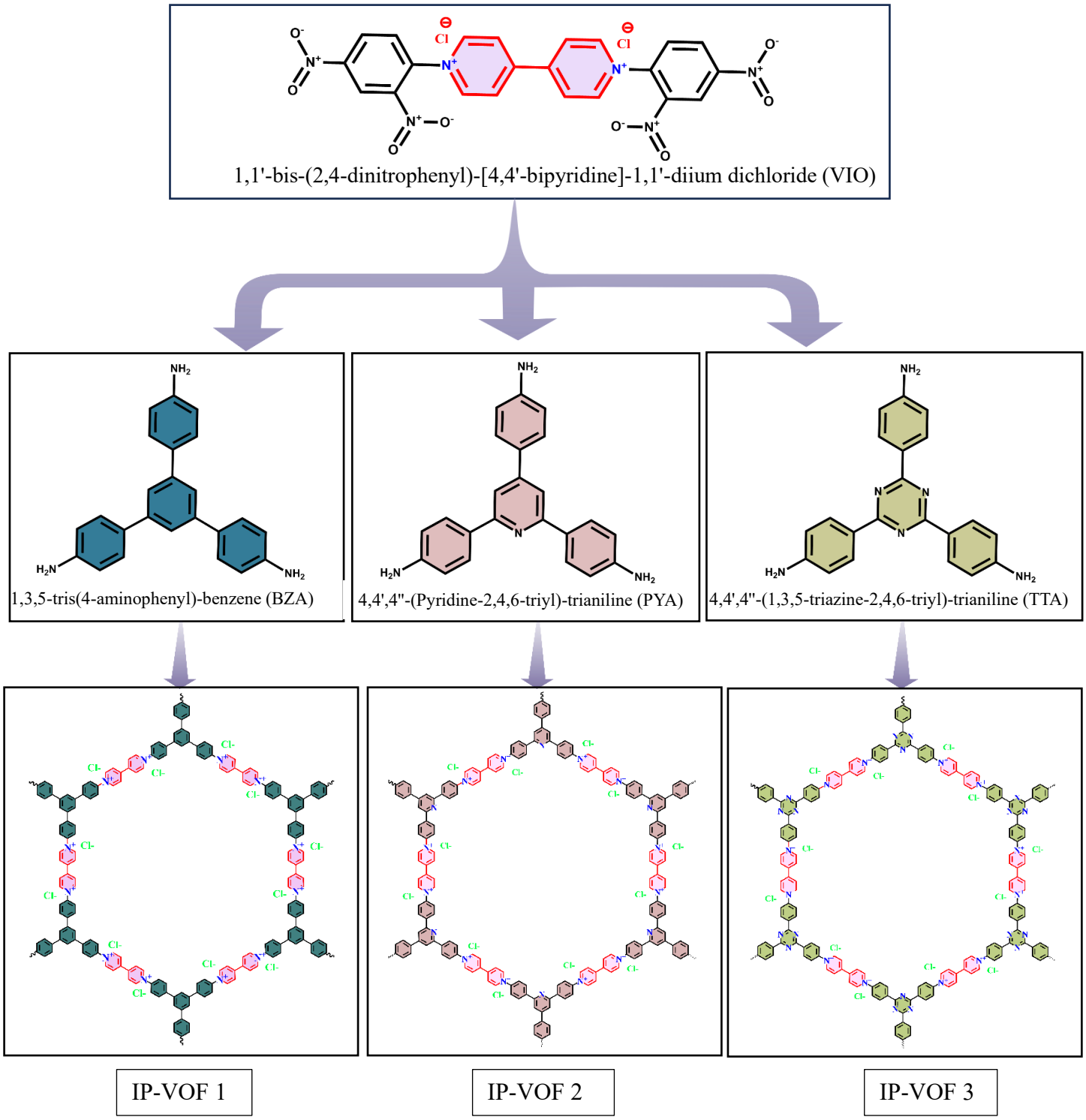

Figure 2.8: Generalized synthesis scheme for IP-VOFs.

3. Results and Discussion

3.1 Characterization

The structural characterizations of these IP-VOFs were performed by Fourier transform infrared (FTIR), solid−state ^{13}C cross-polarization magic-angle-spinning nuclear magnetic resonance (CP-MAS NMR) spectroscopy, thermogravimetric analysis (TGA), low-temperature nitrogen (N_2) gas sorption measurements at 77K, low-temperature carbon dioxide (CO_2) gas sorption measurements at 195K etc., In the analysis of Fourier transform infrared spectroscopy (FT-IR) spectra of IP-VOFs, the disappearance of the characteristic nitro peaks at ∼1343cm^{-1} and ∼1544cm^{-1} in the FTIR spectra of the final product indicates loss of 2,4-dinitroaniline, and disappearance of stretching frequencies of primary NH_2 at ∼3420cm^{-1} and ∼3346cm^{-1} provides evidence for the formation of the expected product. CP-MAS ^{13}C NMR spectra showed broad peaks at 127 and 140 ppm corresponding to the aromatic carbon atoms of the network. Both the Fourier-transform infrared (FTIR) and solid-state ^{13}C cross-polarization magic angle spinning (CP-MAS) nuclear magnetic resonance (NMR) spectra serve as compelling evidence to demonstrate the incorporation of different functional groups, such as triazine and/or pyridine, into their respective VOF structures. In addition, the elemental analysis revealed that the Carbon (C), Hydrogen (H), and Nitrogen (N) content in IP-VOF 1, IP-VOF 2, and IP-VOF 3 closely agreed with the theoretical values. The TGA profiles for all the IP-VOFs under the N_2 atmosphere indicated no significant weight loss up to ~540 °C, further suggesting high thermal stability, however, at temperatures exceeding ~540 °C, it was observed that a consistent weight reduction occurred as a result of the disintegration of the organic components present in the IP-VOFs (Figure 5.6). The IP-VOFs examined in the XPS survey displayed characteristic peaks of elements such as carbon, nitrogen, and chlorine. The C 1s XPS spectra of the IP-VOF 1 to 3 (Figure 3.1 (g,h,i)) displayed peaks within the range of approximately 284.87, 284.88, and 284.94 eV, which corresponded to aromatic carbon bonds (-C=C-) and carbon of C-N. The N 1s XPS spectra of IP-VOF 1 to 3 exhibited peaks at approximately 399.57, 399.28, and 398.18 eV respectively, which corresponded to the N of –C-N bond found in bipyridyl, pyridine, and triazine groups. Similarly, the Cl 2p XPS spectra of IP-VOF

1 to 3 revealed peaks at approximately 197.17, 197.07, and 197.06 eV respectively. The zeta-potential measurement showed that it has a magnitude of +32.1 mV, +37.9 mV, and +31.4 mV on IP-VOF 1, IP-VOF 2, and IP-VOF 3, respectively (Figure 5.8 (a,b,c)). This means that the framework has a positively charged surface, which makes it an excellent adsorbent for Methyl Iodide and Iodine adsorption. In other words, it provides more interaction sites for better adsorption. Powder X-ray diffraction (PXRD) analysis revealed that IP-VOF 1, IP-VOF 2, and IP-VOF 3 are amorphous and the broad peak near θ ~25 represents the π-π stacking of layers of VOFs (Figure 5.9). CO_2 (195 K) gas adsorption-desorption measurement was done and all the IP-VOFs demonstrated type-I adsorption isotherm with high and rapid CO_2 uptake at low partial pressure (Figure 5.11). Moreover, N_2 adsorption isotherm is also performed but IP-VOFs being an ionic porous material showed a notably low amount of N_2 uptake (at 77 K), which is common in ionic materials, these relatively low values may be the result of the pores of the materials being occupied by the existence of chloride counterions within the framework of IP-VOFs and sterically hindering the adsorption of N_2 into the framework (Figure 5.10).

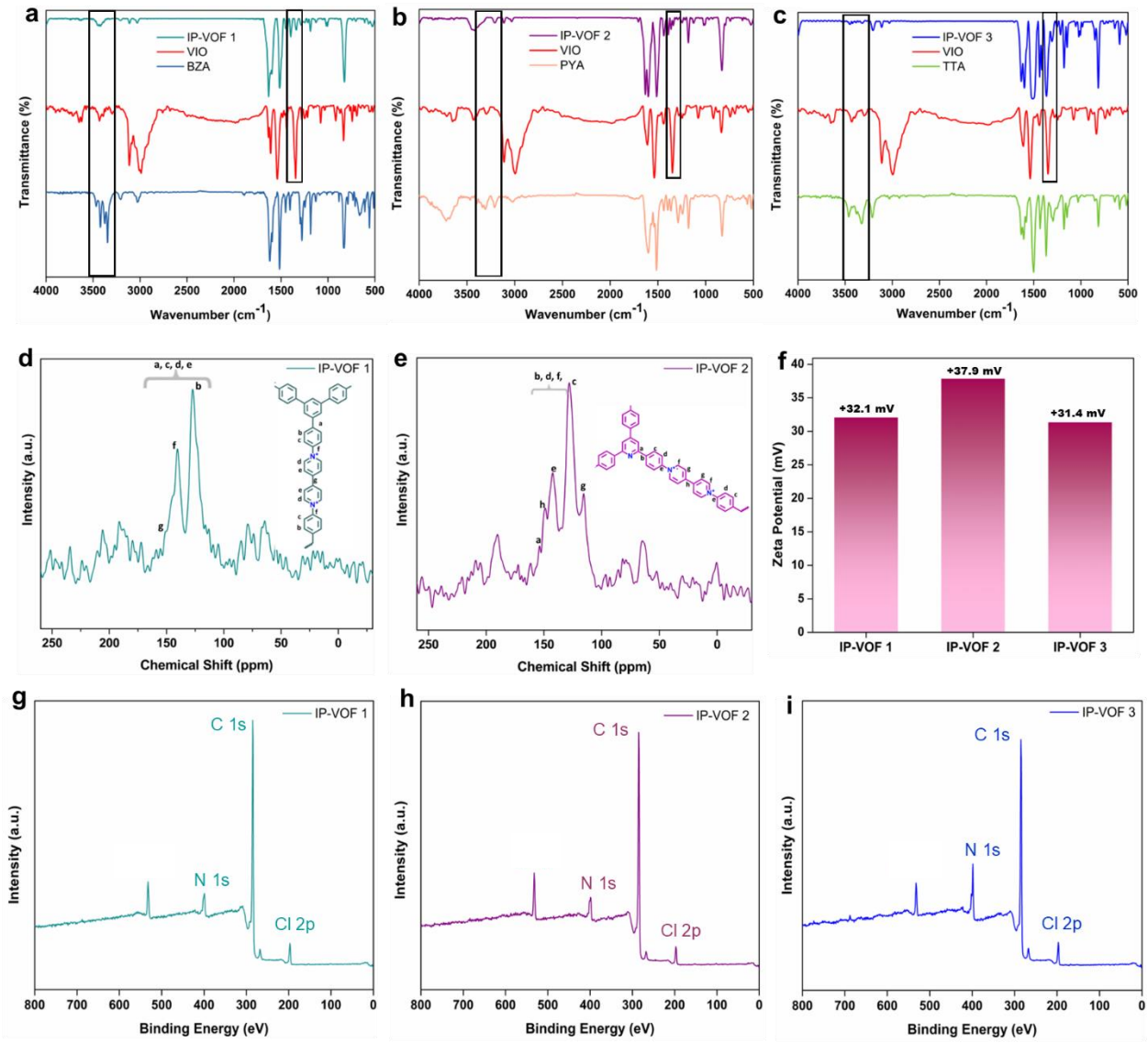

Figure 3.1: FT-IR Spectra of (a) IP-VOF 1, (b) IP-VOF 2, (c) IP-VOF 3, 13C CP-MAS Solid State NMR of (d) IP-VOF 1, (e) IP-VOF 2, (f) Zeta Potential of IP-VOF 1 to 3, X-Ray Photoelectron Spectroscopy (XPS) of (g) IP-VOF 1, (h) IP-VOF 2, (i) IP-VOF 3

Following the structural characterisations, the morphological investigation of the IP-VOFs was carried out using High-Resolution Transmission Electron Microscopy (HR-TEM). The HR-TEM images have unveiled that IP-VOF 1, IP-VOF 2, and IP-VOF 3 display a nanosphere-like morphology, with a diameter varying between 500-800 nm. The elemental composition of the IP-VOFs was determined through elemental analysis (Table 5.2), energy-dispersive X-ray

spectroscopy (EDS) (Figure 5.12), and corresponding mapping (Figure 3.2). It was observed that all the IP-VOFs exhibited the presence of C, N, and Cl elements in a uniform and homogeneous distribution throughout their structures (Figure 3.3).

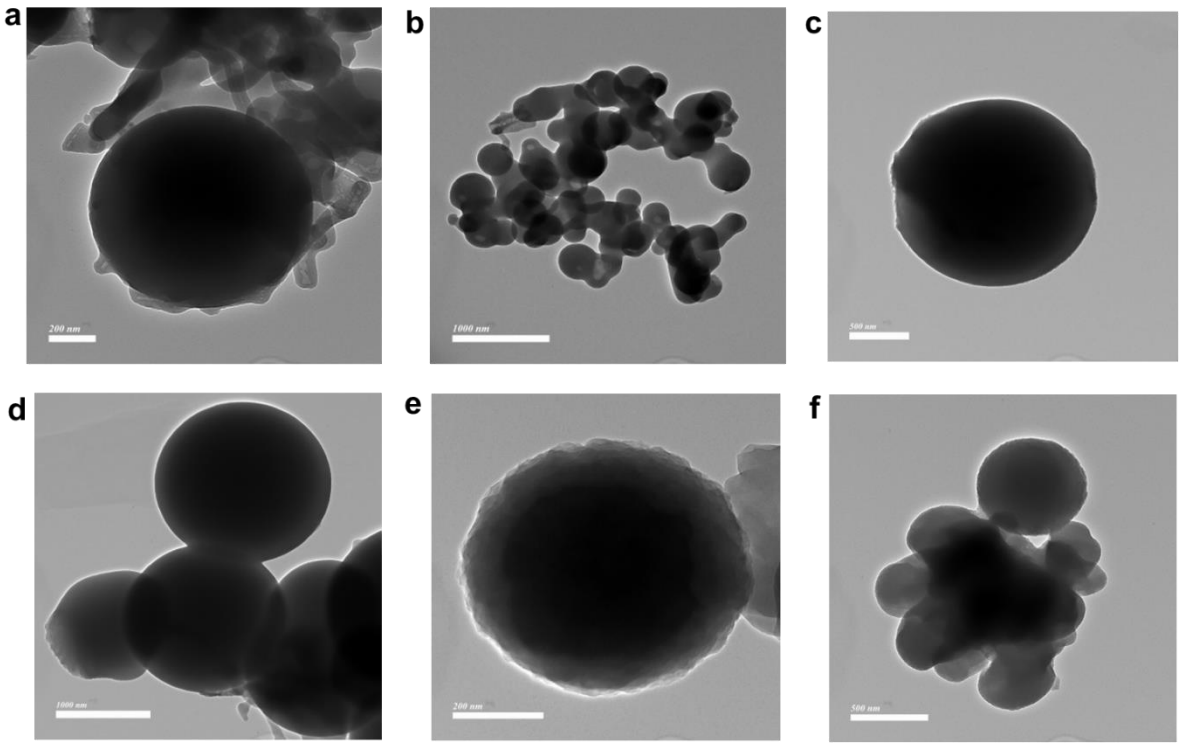

Figure 3.2: Transmission Electron Microscopy (TEM) images of (a,b) IP-VOF 1, (c,d) IP-VOF 2, and (e,f) IP-VOF 3.

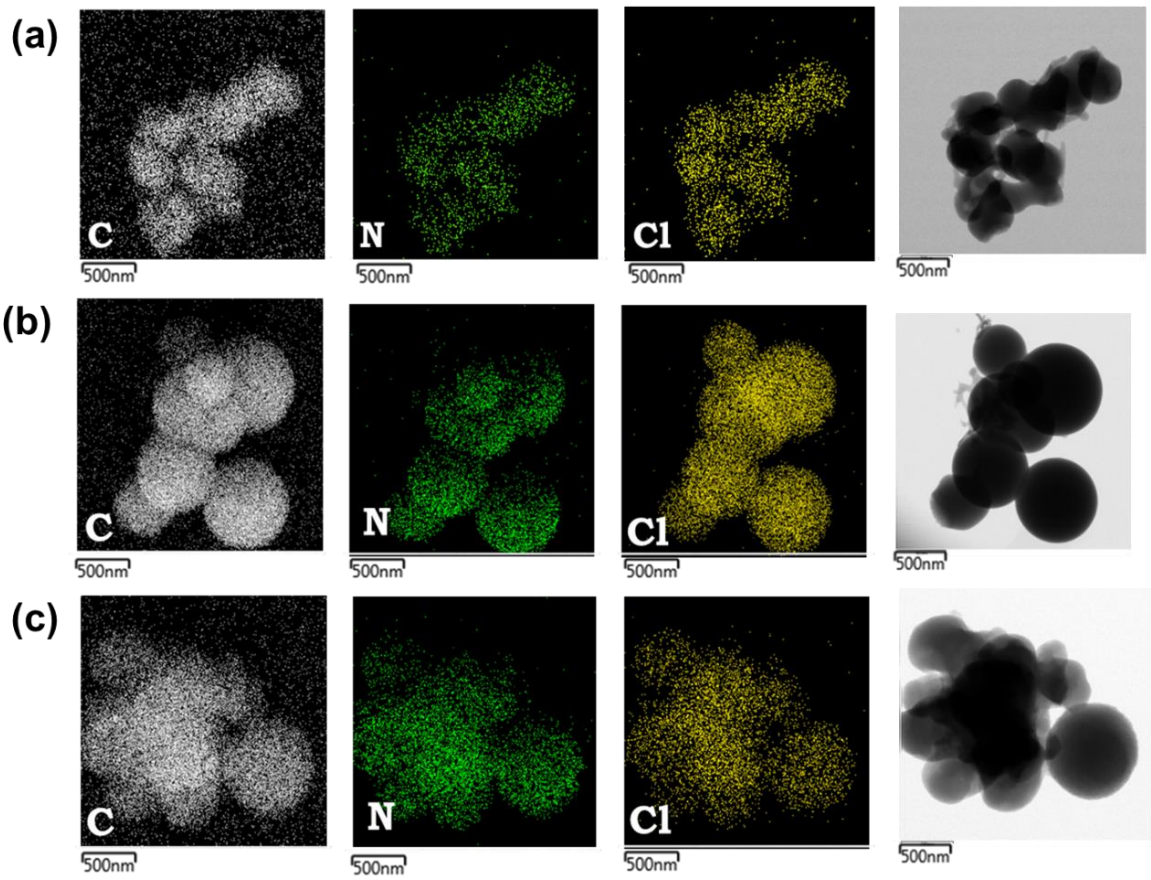

Figure 3.3: Elemental Mapping images from TEM experiment of (a) IP-VOF 1, (b) IP-VOF 2, (c) IP-VOF 3.

3.2 Methyl iodide sorption studies

We conducted both static and dynamic organic iodide sorption experiments after successfully synthesizing and characterizing all IP-VOFs. We aimed to investigate the contribution of framework-integrated functionality towards the effective adsorption of methyl iodide (CH_3I) and Iodine. Drawing upon our prior understanding of the forward dependence of CH_3I and Iodine adsorption on the functionality of porous frameworks, we formulated a hypothesis that among the synthesized VOFs, IP-VOF 3 would manifest the highest organic iodide uptake capacity, attributable to its additional framework-integrated heteroatom functionality. Further, the capacity order should follow as IP-VOF 3 > IP-VOF 2 > IP-VOF 1. Previous studies typically involved CH_3I adsorption in a static, sealed system with CH_3I maintained at (298 K, at 75 °C (348 K), and as well as at 150 °C (423K)), and dynamic capture was also performed at 75 °C. So, the adsorption

capacity was subsequently determined by measuring the mass increase under ambient conditions at room temperature to enable a direct comparison with previously developed adsorbents, we evaluated IP-VOFs using the same experimental setup. It's important to recognize that in this commonly applied evaluation scenario, where the concentration of I_2 is relatively high, the adsorption is primarily influenced by the intermolecular interactions of I_2. Therefore, the adsorbent's pore volume, as well as the characteristics of the binding sites, play a major role in determining the capacity.

The present study involved the gravimetric measurement of organic iodide uptake by IP-VOFs at 348 K under ambient pressure, employing three parallel experimental setups, (Figure 5.1). The kinetics of the process were investigated by measuring the uptake at various time intervals. The change in weight of the IP-VOFs after CH_3I adsorption was then plotted against time. The experimental results indicate that the three IP-VOFs exhibit notable CH_3I capture capacity with rapid uptake kinetics. Nonetheless, it is important to note that the degree of uptake varied among the VOFs under investigation. We encountered an interesting result at 348 K and 423K which is different from the studies on adsorption of methyl iodide. Notably, it was found that the adsorption capacity of CH_3I at 348 K reached 2.12 g. g^{-1} at 24 h, and the maximum uptake amount was 3.47 g. g^{-1} within 72 h for IP-VOF 2. Surprisingly, for IP-VOF 1 and IP-VOF 3, the saturation adsorption capacity of CH_3I was found to be 1.61, and 2.71 g. g^{-1}, respectively within 72 h under the same conditions (Figure 3.4 (a)). Furthermore, the adsorption study of CH_3I vapour was conducted at different temperatures, including ambient temperature (298 K) and industrially relevant temperature (423 K), to investigate the temperature dependence of the adsorption process. At 298K, IP-VOF 1 to 3, exhibited 0.81, 0.82, and 0.85 g. g^{-1} respectively. Moreover, at 423K, we encountered a surprising result, IP-VOF 1 to 3 showed 3.27, 4.92, and 2.86 g. g^{-1} uptake capacity respectively (Figure 3.4 (b)). IP-VOF 2 displayed the highest reported to date at both 348 K and 423 K. This is due to the higher reactivity and basicity of pyridine as compared to triazine in IP-VOF 3. However, the order of these IP-VOFs' capacities was found as IP-VOF 1 < IP-VOF 3 < IP-VOF 2 (at 348 K). And at 423 K the order follows as IP-VOF 3 < IP-VOF 1 < IP-VOF 2.

The absorption of iodine was also studied using a consistent setup at 348K (Figure 5.2), revealing that IP-VOF 1 to 3 exhibited notable uptake capacity for Iodine. Specifically, the measurements showed 4.91, 5.47, and 5.53 g. g^{-1}, respectively, which can be attributed to its higher N content

promoting the initial adsorption of I_2. However, the order of these capacities of all the IP-VOFs was found as almost similar to the previous studies IP-VOF 1 < IP-VOF 2 < IP-VOF 3. Absorption amounts are significantly higher than most of the benchmark materials used for Iodine and CH_3I adsorption under the same conditions. The CH_3I@IP-VOFs were shown to maintain their weight with minimal loss after 7 days, indicating that the absorption is not caused by surface condensation but rather by the strong interaction between the structure of the IP-VOFs and CH_3I molecules. The retention efficiency of all three VOFs for methyl iodide (Figure 5.18), as well as Iodine (Figure 5.19), is more than 85%, which makes this material suitable for practical use. The time-dependent study of methyl iodide and iodine uptake was fitted in a pseudo-second-order kinetic equation and it fits well with a correlation coefficient of R^2 =0.99 (Figure 3.13).

In nuclear waste or off-gas streams, CH_3I vapour coexists with moisture, nitric acid, and nitrogen oxides (i.e., NO_2). Therefore, practical adsorbents must be stable in water and highly acidic conditions, so we tested the adsorbents in moist conditions as well as in the presence of nitric acid. In addition, the presence of water vapour only caused a slight decrease in the CH_3I uptake, indicating that they are tolerant to moisture, which is important for practical applications. To better understand the effectiveness of adsorbents in practical applications, it is more relevant to test their adsorption behaviour at low concentrations of organic iodides, which are usually below 200 ppm in the off-gas stream. To assess the potential of IP-VOFs for practical use, we examined their capacity to adsorb CH_3I under dynamic conditions using a home-built setup (Figure 5.3, 5.4) to compare the developed IP-VOFs with benchmark adsorbents directly, we conducted dynamic adsorption at 75 °C with CH_3I in N_2 flow, and got the uptake capacities as 0.74, 1.11, 0.62 g. g^{-1} for IP-VOF 1,2, and 3 respectively (Figure 3.5).

The introduction of water vapor into the feed stream resulted in a decrease in the CH_3I adsorption capacity which indicates competitive adsorption between H_2O and CH_3I. The reason for this is that the adsorption of CH_3I primarily occurs on N sites, which also interact with H_2O molecules. The dynamic adsorption measurements reveal that IP-VOFs have similar uptake capacity trends. This outcome is consistent with the results of the static adsorption experiments.

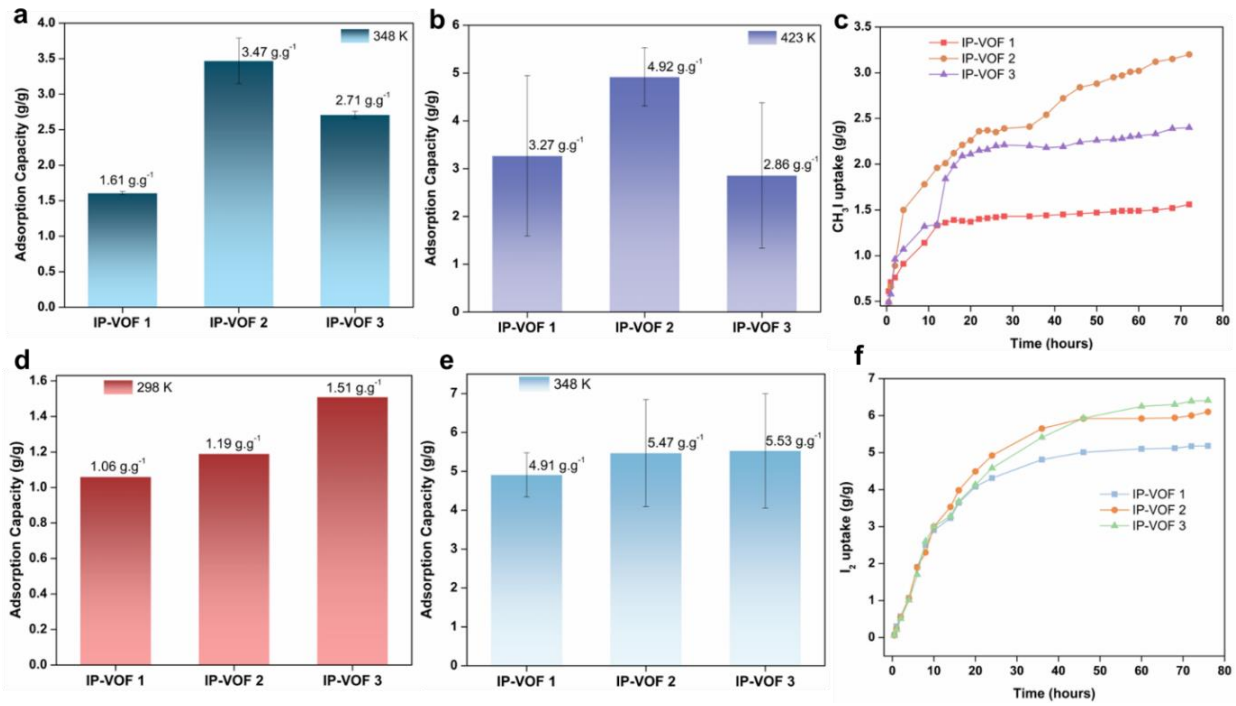

Figure 3.4: (a,b) CH_3I adsorption capacities of IP-VOF 1 to 3 at 348 K and at 423 K respectively, within 72 h, (c) CH_3I adsorption capacities of IP-VOF 1 to 3, as a function of time at 348 K under static condition within 72 h, (d,e) I_2 adsorption capacities of IP-VOF 1 to 3 at 298K and at 348 K respectively, within 72 h, (f) I_2 adsorption capacities of IP-VOF 1 to 3, as a function of time at 348 K under static condition.

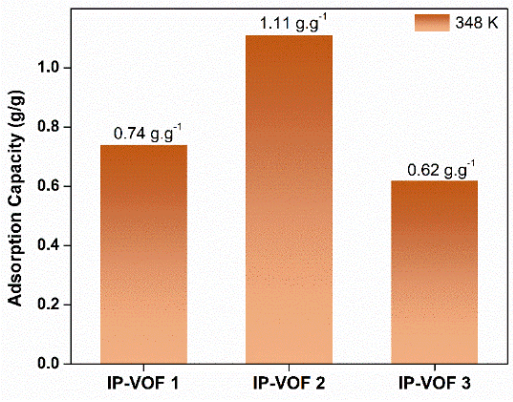

Figure 3.5: CH_3I adsorption capacities of IP-VOF 1, IP-VOF 2, and IP-VOF 3 in dynamic vapour phase capture study at 348 K.

3.3 Post-Capture Characterization

The adsorption of methyl iodide on IP-VOFs was analyzed through Fourier transform infrared spectroscopy (FT-IR) spectra, which revealed a change in the intensity and shift of the characteristic bands of C=C, and C=N bonds. Additionally, a new band at approximately 936 cm^{-1} [6] and 770 cm^{-1} indicated the formation of a new C–N bond due to methylation reaction and monosubstituted C-H bending, respectively (Figure 3.6 (a,b,c)). It is important to note that there were no changes in the bands of C=C at 1630–1596 cm^{-1} upon CH_3I adsorption except for minor peak shifts and slightly reduced intensity. These results support the conclusion that CH_3I molecules are specifically bonded to nucleophilic N sites through N-methylation reactions, rather than being adsorbed on the benzene, triazine, or pyridine cores. Solid-state ^{13}C NMR spectra revealed that the chemical shifts of all carbon atoms in IP-VOFs changed to a certain extent after the adsorption of methyl iodide, and a new peak appeared at ~57 ppm to ~59 ppm (Figure 3.5), which was attributed to the C atoms of CH_3I molecules, indicating the successful grafting of CH_3I into the structure of the IP-VOFs. Moreover, the Raman spectra of CH_3I@IP-VOFs showed distinct bands at ~109.6 cm^{-1}, and ~164.0 cm^{-1} following methyl iodide adsorption (Figure 3.6 (g,h,i)) [6,7]. Furthermore, the adsorption of Iodine on IP-VOFs was analyzed by the Raman spectra, and I_2@IP-VOF showed distinct bands at ~106.6 cm^{-1}, and ~169.7 cm^{-1} following iodine adsorption (Figure 3.6 (d,e,f)), indicating strong charge-transfer interaction of iodine with IP-VOFs and generation of a multitude of anionic polynuclear iodide species. Among them, the band at ~106.6 cm^{-1} can be assigned to the stretching vibration of I^{3-} whereas, the band at 169.7 cm^{-1} is attributed to the stretching vibration of I^{5-} polyiodide species, suggesting that electron-deficient I_2 molecules interacted with various sites throughout the entire π-electron conjugated framework [5,15]. It was observed through the thermogravimetric analysis of methyl iodide loaded adsorbent (CH_3I@IP-VOFs) that after reaching a temperature of 150°C, there was a gradual decrease in mass that signified the loss of adsorbed CH_3I (Figure 5.17 (a,b,c)). This also indicated the strong interaction of adsorbed methyl iodide with the ionic polymers as bare methyl iodide is volatile and evaporates even at room temperature. And in the case of iodine-loaded IP-VOFs (I_2@IP-VOFs) after reaching a temperature of 120°C, there was a gradual decrease in mass that signified the loss of adsorbed Iodine (Figure 5.17 (d,e,f)). The High-Resolution Transmission Electron Microscopy (HR-TEM) images (Figure 5.14) and elemental mapping data have provided a detailed insight into the distribution of iodine and methyl iodide over IP-VOFs. The results show that the absorption of

excessive I_2 and CH_3I by the IP-VOFs has led to a homogenous distribution of iodine over the framework (Figure 3.7, 3.8).

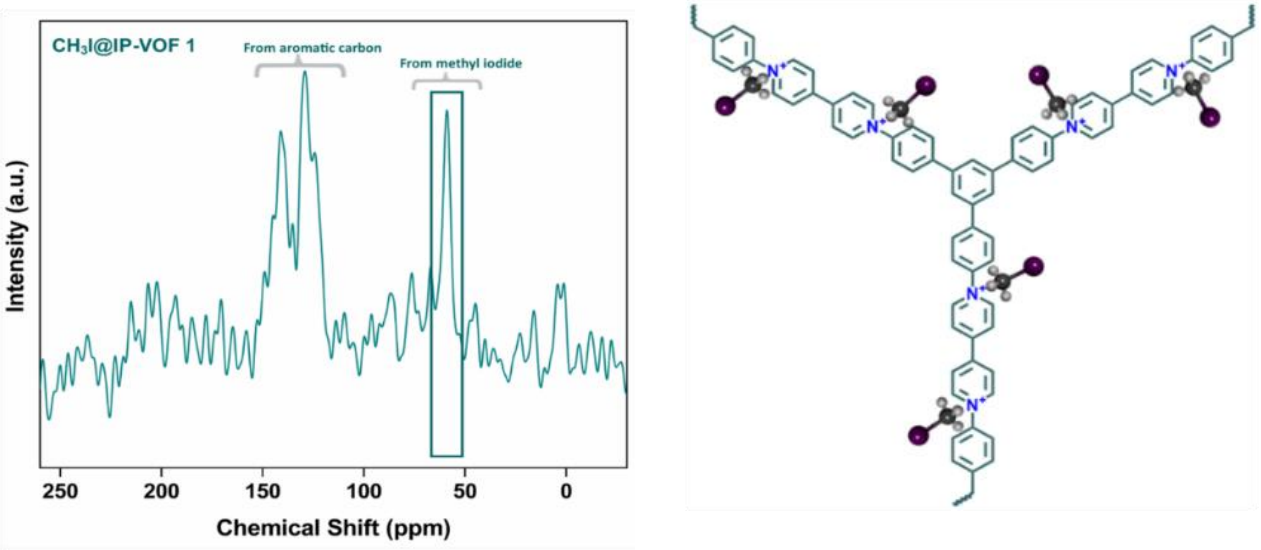

Figure 3.6: ^{13}C CP-MAS solid state NMR of CH_3I@IP-VOF 1

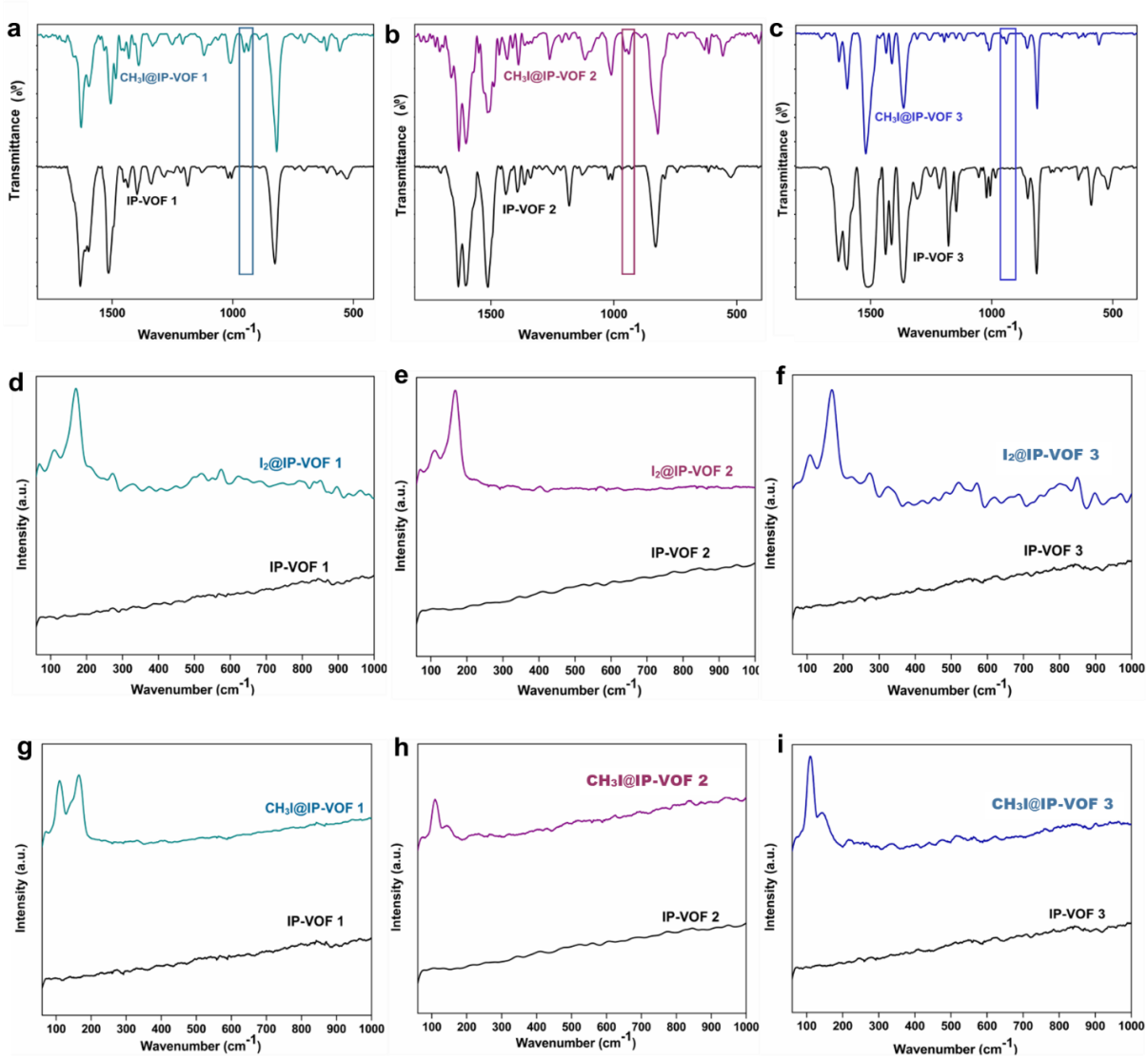

Figure 3.7: FT-IR spectra of (a) CH_3I@IP-VOF 1, (b CH_3I@IP-VOF 2, (c) CH_3I@IP-VOF 3, Raman spectra of (d) I_2@IP-VOF 1, (e) I_2@IP-VOF 2, (f) I_2@IP-VOF 3, Raman spectra of (g) CH_3I@IP-VOF 1, (h) CH_3I@IP-VOF 2, (i) CH_3I@IP-VOF 3.

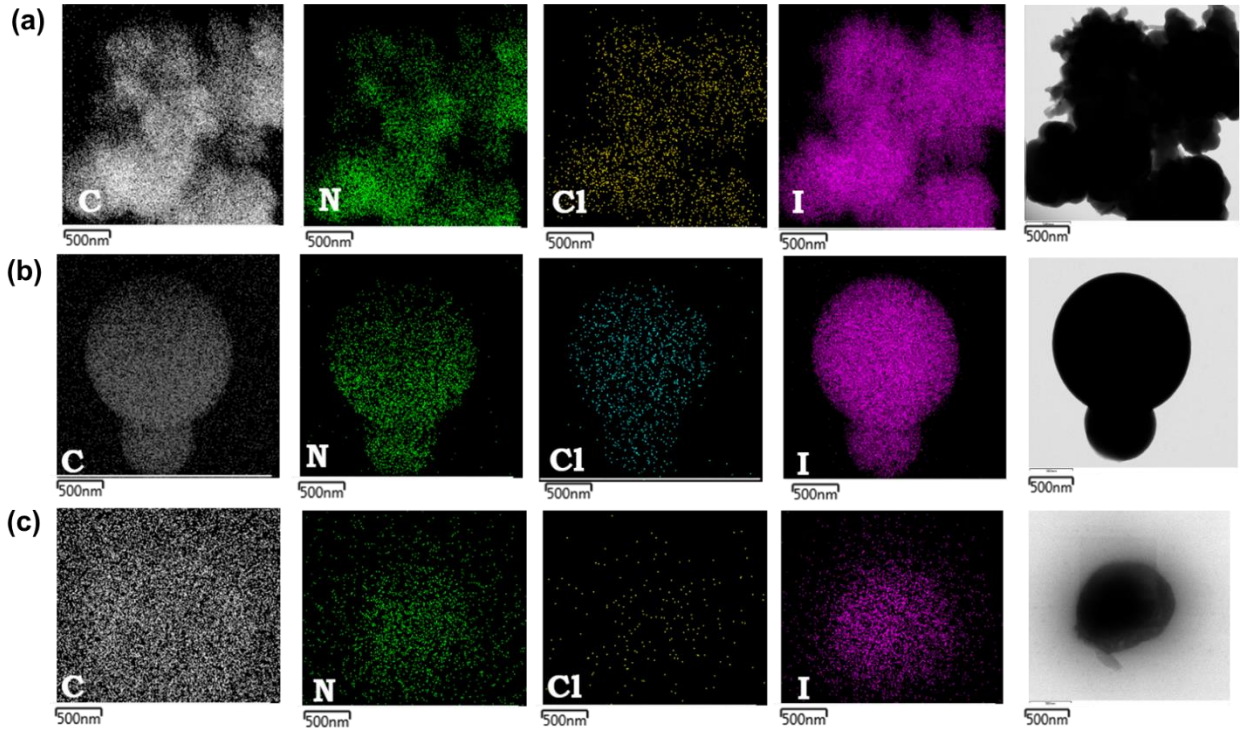

Figure 3.8: Elemental Mapping images from TEM experiment of (a) CH_3I@IP-VOF 1, (b) CH_3I@IP-VOF 2, (c) CH_3I@IP-VOF 3.

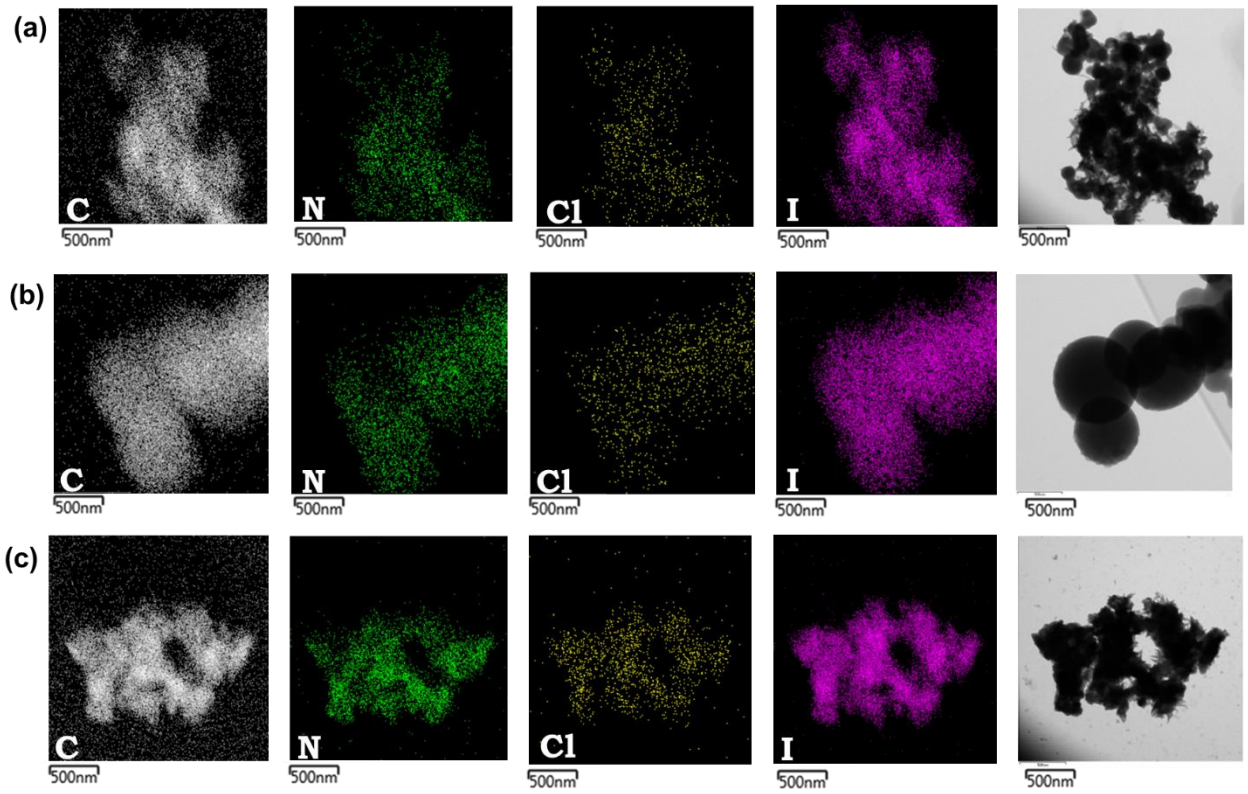

Figure 3.9: Elemental Mapping images from TEM experiment of (a) I_2@IP-VOF 1, (b) I_2@IP-VOF 2, (c) I_2@IP-VOF 3.

3.4 Recovery and Recyclability

The adsorption capacity of CH_3I@IP-VOFs can be restored by using ethanol to extract methyl iodide. When IP-VOFs become fully saturated with Methyl Iodide, immersion in ethanol triggers a spontaneous CH_3I desorption process, which is further accelerated with the aid of sonication. Extracting the adsorbents with ethanol is a widely adopted and efficient method for restoring them after adsorption, due to the reversible N-methylation reaction facilitated by protic solvents. After the desorption process, the solution of ethanol containing methyl iodide can be subjected to further processing to separate methyl iodide from ethanol. This can be achieved by using fractional distillation, as there is a significant difference between the boiling points of methyl iodide and ethanol as the boiling point of methyl iodide is 42 °C, whereas the boiling point of ethanol is 78 °C.

To recover Iodine from Iodine-loaded adsorbent (I_2@IP-VOFs) and to restore its adsorption efficiency for further use it was heated in a closed chamber at a temperature of approximately 150 °C (Figure 5.20). The iodine vapour generated from the compound as a result of heating was then condensed in a separate glass flask, which was kept in an ice-cool bath for a certain time. It was observed that solid crystals of iodine had formed and condensed on the surface of the glass flask (Figure 5.21). These solid iodine crystals were then collected in a separate storage vial and we were able to recover 85.1% of solid Iodine from the I_2@IP-VOFs. To regenerate the adsorbent compound, it was immersed in hexane, which dissolved nearly all the remaining iodine and after activation IP-VOFs were used for the next cycle of adsorption [5].

4. Conclusion

In summary, we have successfully produced IP-VOFs using Zincke's reaction and conducted a detailed analysis of its structure and optical properties to gain a better understanding of its characteristics. Through this, we have conducted a systematic investigation to comprehend the function of framework-integrated N-heterocyclic or heteroatomic nucleophilic functionalities in a series of isostructural chemically stable porous IP-VOFs towards selective and effective sequestration of organic iodide vapour. The bipyridine group into the building block of the framework serves for the capture of both iodine gas through enhanced electron-pair effect and methyl iodide via the methylation reaction and electrostatic interaction. Out of the series, IP-VOF 2, which contains bipyridyl and pyridine groups, has been found to exhibit a remarkably high capacity for adsorbing CH_3I in various relevant temperatures, including dry, humid, and acidic conditions, in both static and dynamic phases. This is due to the higher reactivity and basicity of pyridine as compared to triazine in IP-VOF 3, thus making it an excellent adsorbent for real-time radionuclide sequestration. When tested at 348 K and 423 K, in both static and dynamic conditions, IP-VOF 2 has been found to possess a CH_3I sorption capacity that exceeds that of most reported adsorbents. For the iodine sequestration study, IP-VOF 3 performed the best due to its high number of nucleophilic N sites that enhance the electron-pair effect, resulting in greater iodine adsorption. These results advocate the practical utility of IP-VOF 2 for real-life applications, especially in nuclear fuel rod reprocessing plants that require efficient and reliable ROI adsorption capacities. Furthermore, we believe that these findings will help to accelerate the development of adsorbents based on ionic polymers.

5. Appendix

5.1 Vapor Phase Static Capture Study

To measure the static adsorption capacity, about 15 mg of activated IP-VOF sample was weighed and placed in a small glass vial which is in the Teflon autoclave vial. The vial was then exposed to Methyl iodide (approximately 1 mL) or molecular Iodine at 75°C (348 K) or 150°C (423 K) in a closed system for their respective measurements. After 72 hours of adsorption, the glass vial was taken out, allowed to cool to room temperature, and weighed again. The uptake capacity of the sample was determined by calculating the difference in weight of the glass vial before and after adsorption.

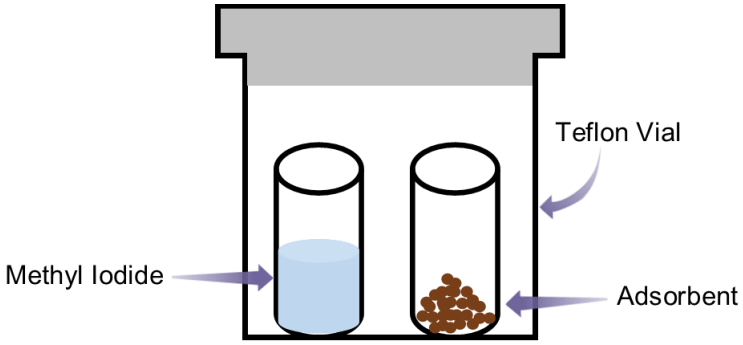

Figure 5.1: Schematic diagram of the experimental setup for vapour phase static CH_3I capture.

Figure 5.2: Schematic diagram of the experimental setup for vapour phase static I_2 capture.

5.2 Vapour Phase Dynamic Capture Study

To study the adsorption of gaseous methyl iodide in a dynamic system, a homemade setup was used. Initially, around 50mg of activated IP-VOF sample was filled into a glass column. Glass wool was used to fill the void space of both ends, creating an adsorption cell. The adsorption cell was then placed in an oven along with a separate chamber that contained methyl iodide. Both chambers were heated to 75 ℃ for a specific period. To blow the methyl iodide vapour into the adsorption cell, a nitrogen flow of 5 cm^3 /min was passed through the methyl iodide vapour generator (inlet). The effluent from the adsorption cell was treated with 1 M NaOH solution. The adsorption capacity of methyl iodide was calculated by measuring the weight difference of glass tubes before and after adsorption. A similar method was used to perform the study in the presence of nitric acid vapour. HNO_3 was placed in a separate glass vial along with the methyl iodide vial to capture dynamic methyl iodide.

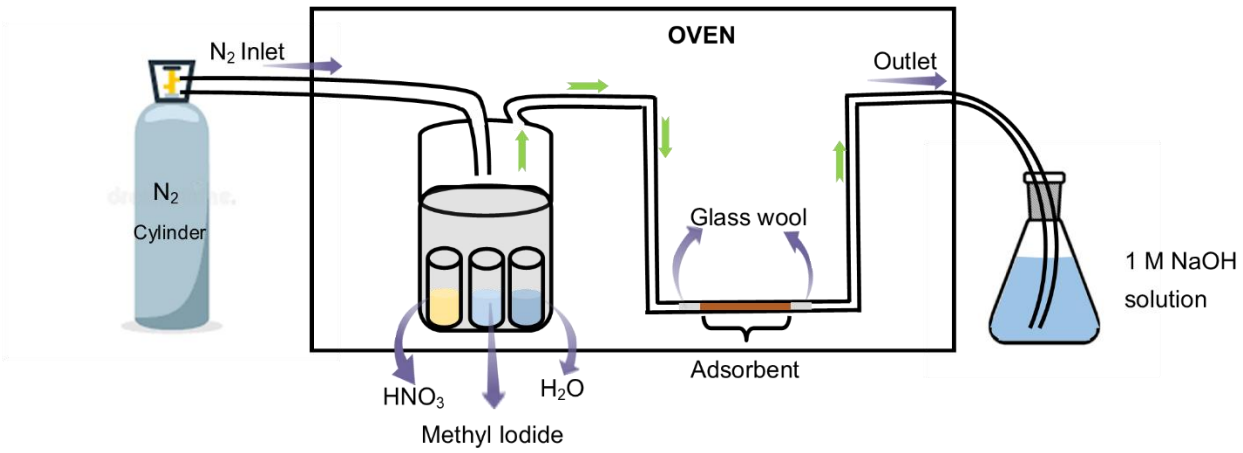

Figure 5.3: Schematic diagram of the experimental setup for vapour phase dynamic CH_3I capture study.

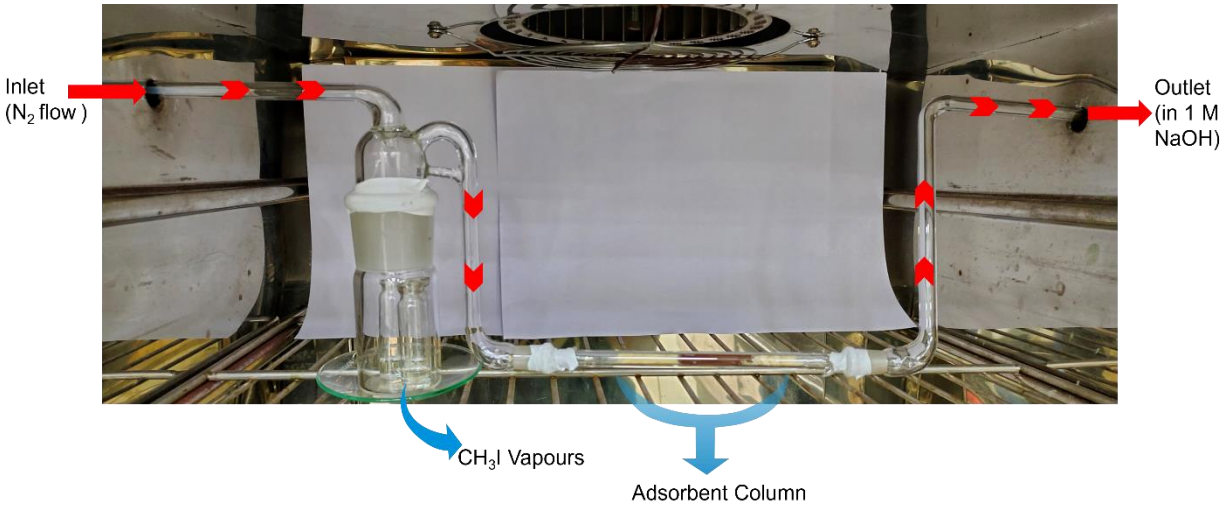

Figure 5.4: Digital image of the experimental setup for vapour phase dynamic CH_3I capture study.

Figure 5.5: Digital image of the adsorbent column used in vapour phase dynamic CH_3I capture study.

5.3 Capacity Calculation

The maximum static capture capacity was measured by the weight increment of the adsorbents. The static CH_3I vapour capture uptake (c, g· g^{-1}) at a certain time was calculated by the equation:

$$c= m_t-m_0/ m_1-m_0$$

where 'c' ($g.g^{-1}$) denotes the static CH_3I vapour capture uptake at time t,

m_t (g) denotes the weight of the vial containing adsorbents at time t,

m_1 (g) denotes the weight of the vial containing adsorbent before sorption,

m_0 (g) denotes the weight of the empty vial for adsorbents.

5.4 Kinetic Data Fitting

The adsorption kinetics were further quantified utilizing a pseudo-second-order model from which the apparent rate constant k_{obs} can be obtained using the following equation:

$$t/q_t = t/q_e + 1/k_{obs}q_e^2$$

Where, q_t and q_e are the adsorbate uptakes (gm adsorbate per gm of VOFs) at time t (hour) and at equilibrium, respectively, and k_{obs} is an apparent second-order rate constant (g. g^{-1}. $hour^{-1}$). The rate constant k_{obs} can be calculated from the intercept and slope of the plot of t/q_t against t. (Figure 5.13)

Compound	**q_e (g. g^{-1})**	**k_{obs} ($hour^{-1}$. g. g^{-1})**
CH_3I@IP-VOF 1	1.5556	0.2775
CH_3I@IP-VOF 2	3.3990	0.0348
CH_3I@IP-VOF 3	2.5031	0.0844
I_2@IP-VOF 1	6.3601	0.0106
I_2@IP-VOF 2	8.0640	0.0058
I_2@IP-VOF 3	8.9847	0.0042

Table 5.1: Fitting data of Methyl Iodide and iodine-loaded IP-VOFs

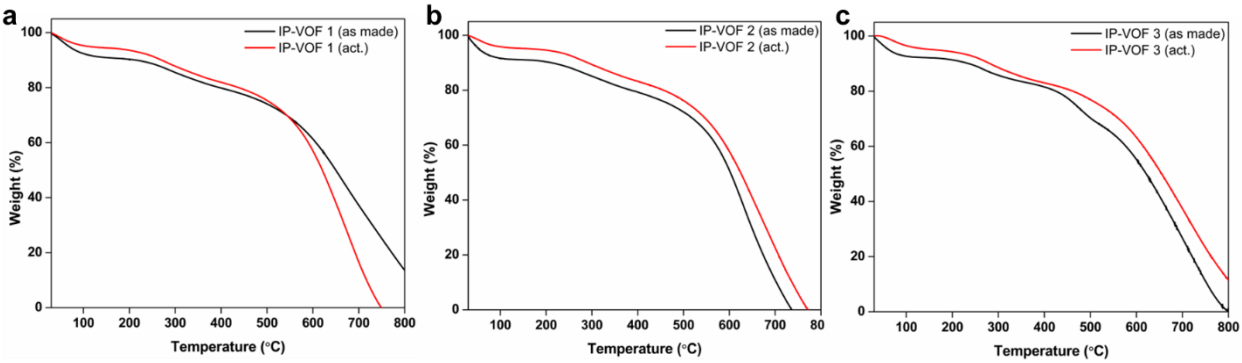

Figure 5.6: Thermogravimetric Analysis (TGA) of (a) IP-VOF 1, (b) IP-VOF 2, (c) IP-VOF 3.

	Experimental		
Compound	**C (%)**	**N (%)**	**H (%)**
IP-VOF 1	67.97	8.44	6.04
IP-VOF 2	64.16	11.97	5.04
IP-VOF 3	61.90	15.28	4.96

Table 5.2: Elemental Analysis Data of IP-VOF 1 to 3.

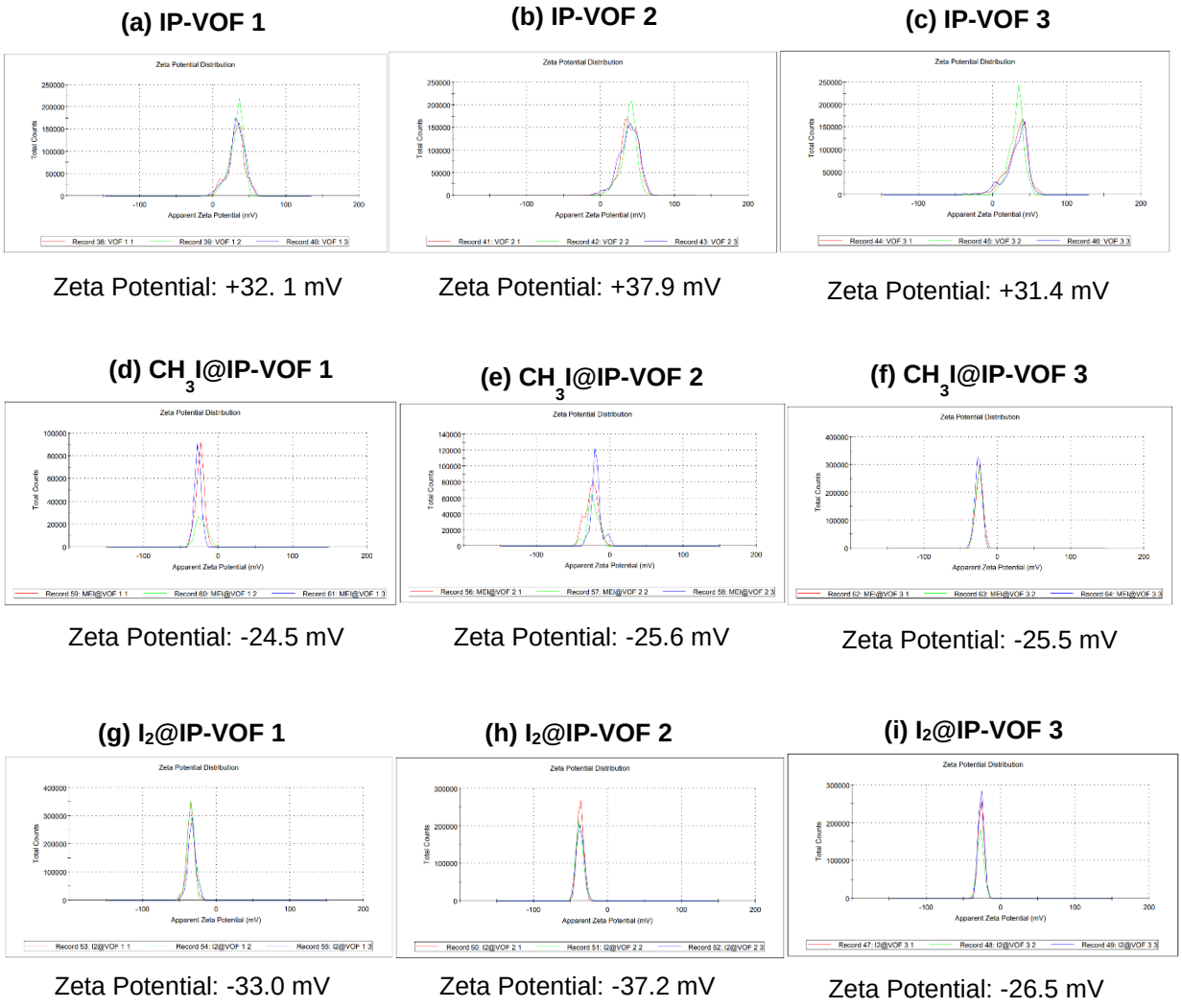

Figure 5.8: Zeta Potential Measurements of (a, b,c) IP-VOF 1 to 3, (d,e,f) CH_3I@IP-VOF 1 to 3, (g,h,i) I_2@IP-VOF 1 to 3

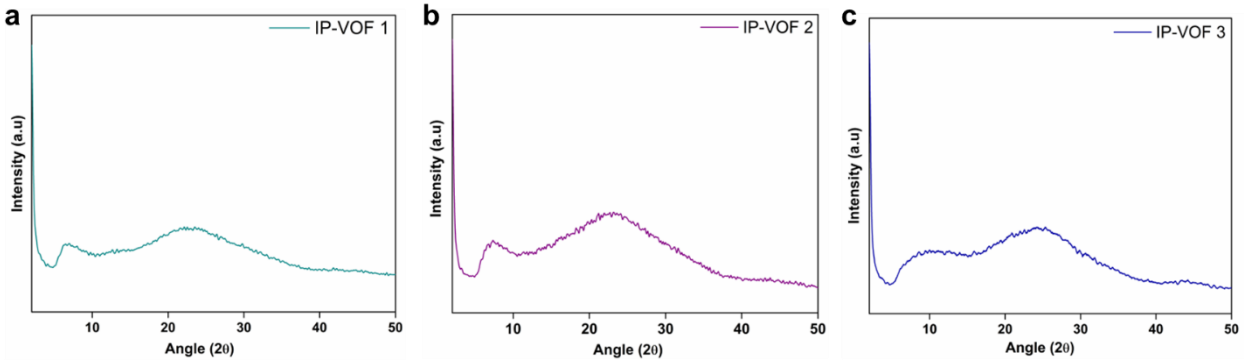

Figure 5.9: Powder X-Ray Diffraction (PXRD) of (a) IP-VOF 1, (b) IP-VOF 2, (c) IP-VOF 3

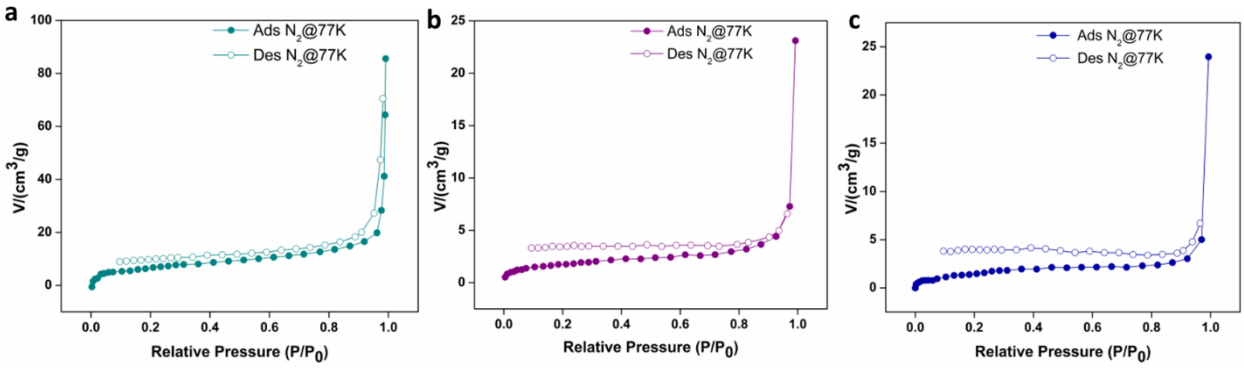

Figure 5.10: N_2 Adsorption-Desorption Isotherm of (a) IP-VOF 1, (b) IP-VOF 2, and (c) IP-VOF 3.

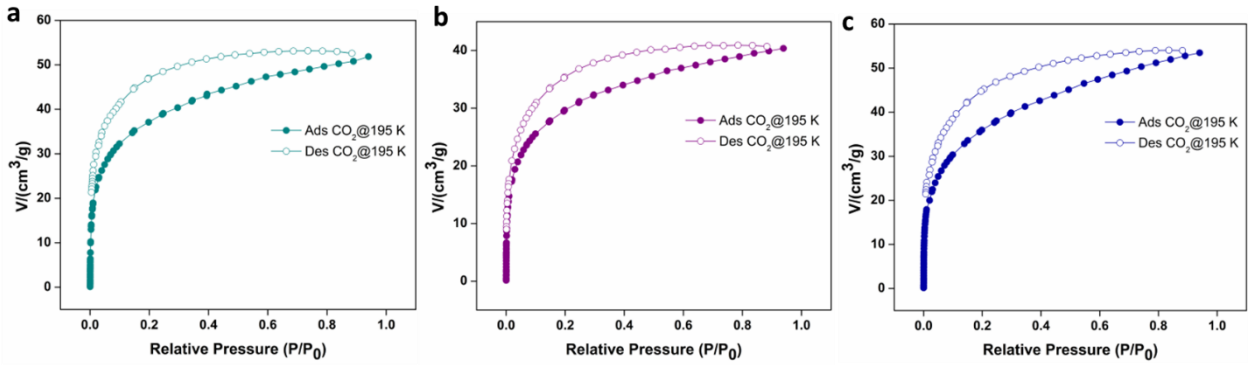

Figure 5.11: CO_2 Adsorption-Desorption Isotherm of (a) IP-VOF 1, (b) IP-VOF 2, and (c) IP-VOF 3.

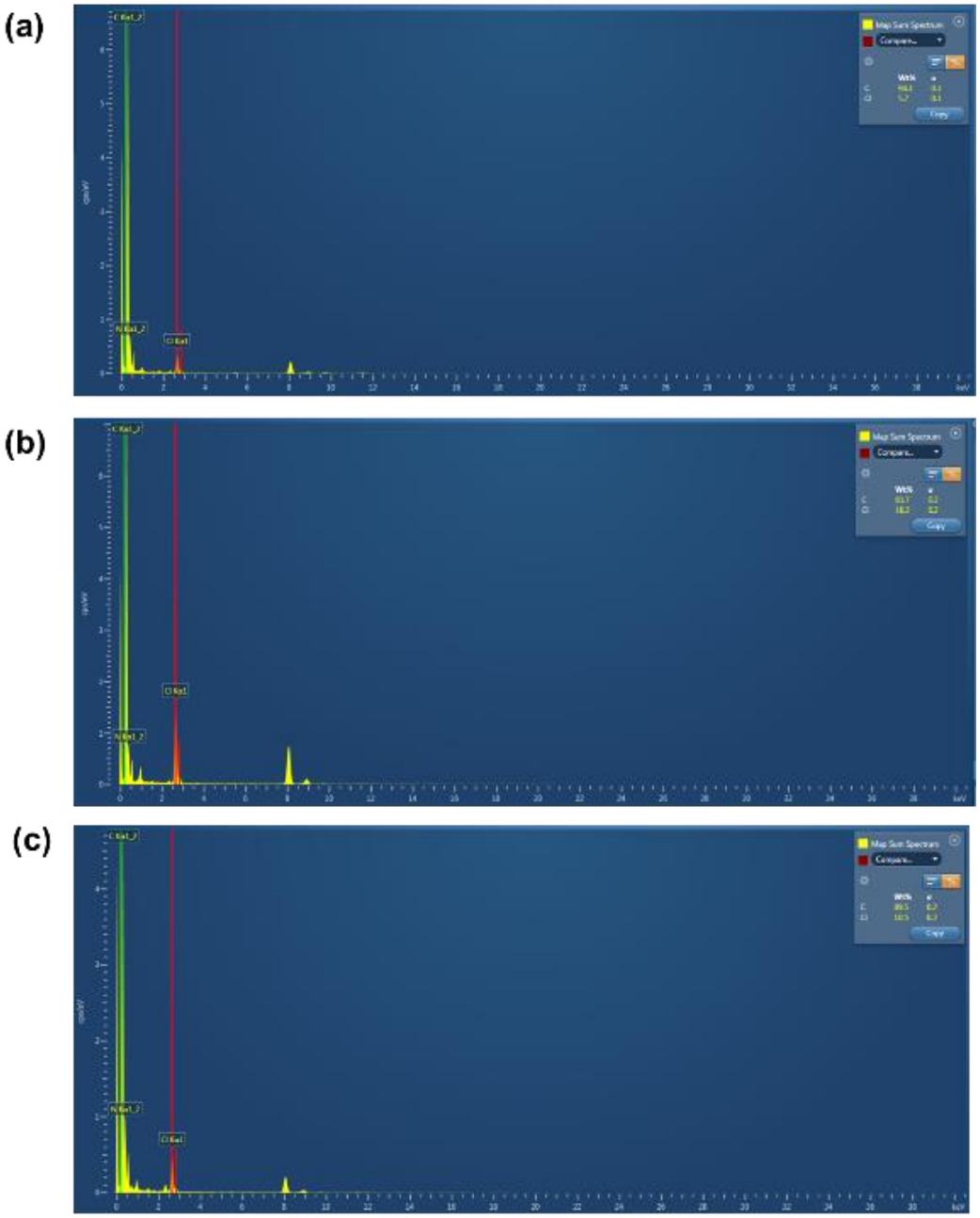

Figure 5.12: Energy-dispersive X-ray spectroscopy (EDS) data from HR-TEM experiment of (a) IP-VOF 1, (b) IP-VOF 2, (c) IP-VOF 3.

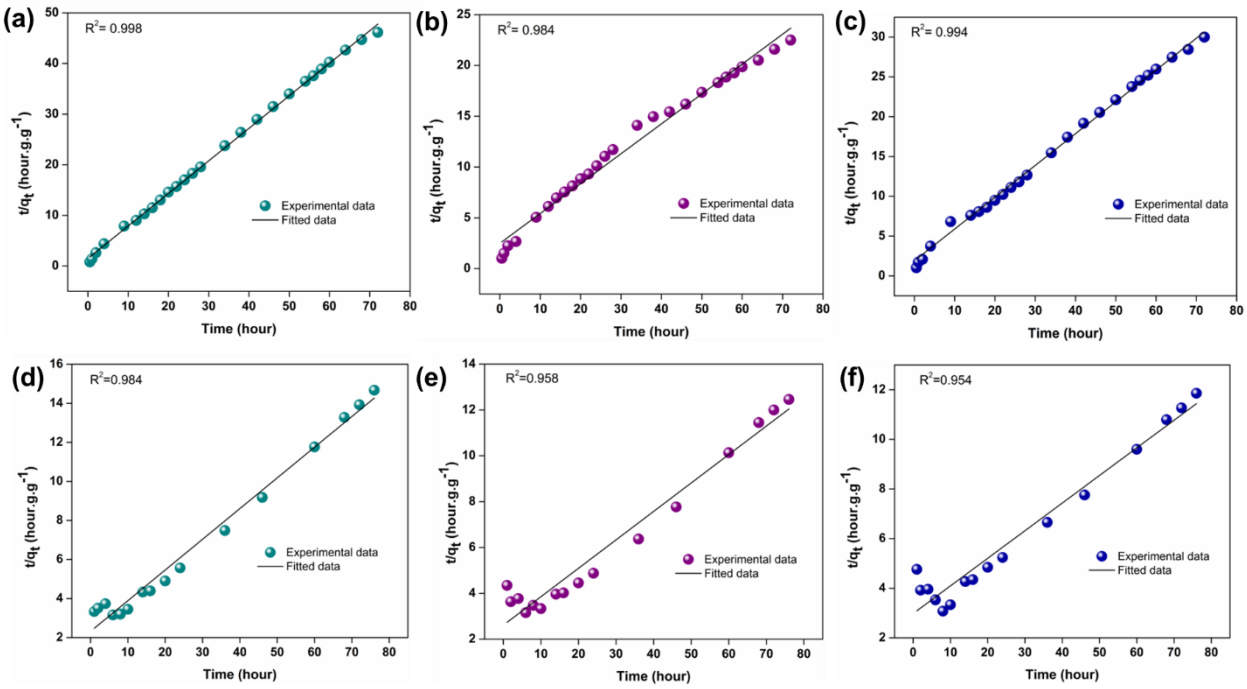

Figure 5.13: Pseudo-second-order kinetic model fitting data of (a) IP-VOF 1, (b) IP-VOF 2, and (c) IP-VOF 3 for CH_3I adsorption.

Pseudo-second-order kinetic model fitting data of (d) IP-VOF 1, (e) IP-VOF 2, and (f) IP-VOF 3 for I_2 adsorption.

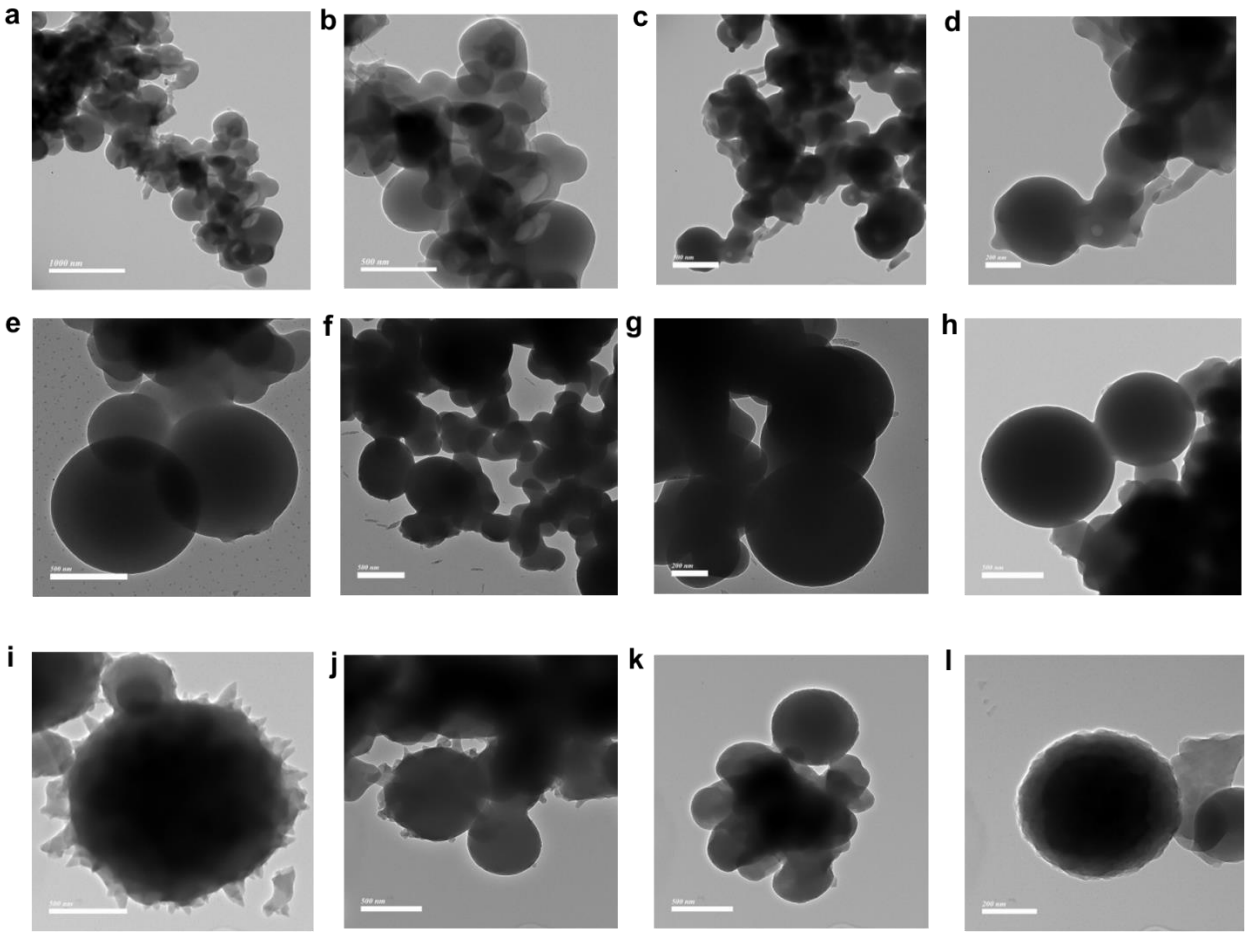

Figure 5.14: High-Resolution Transmission Electron Microscopy (HR-TEM) images of (a,b) I_2@IP-VOF 1, (c,d) CH_3I@IP-VOF 1, (e,f) I_2@IP-VOF 2, (g,h) CH_3I@IP-VOF 2, (i,j) I_2@IP-VOF 3, (k,l) CH_3I@IP-VOF 3.

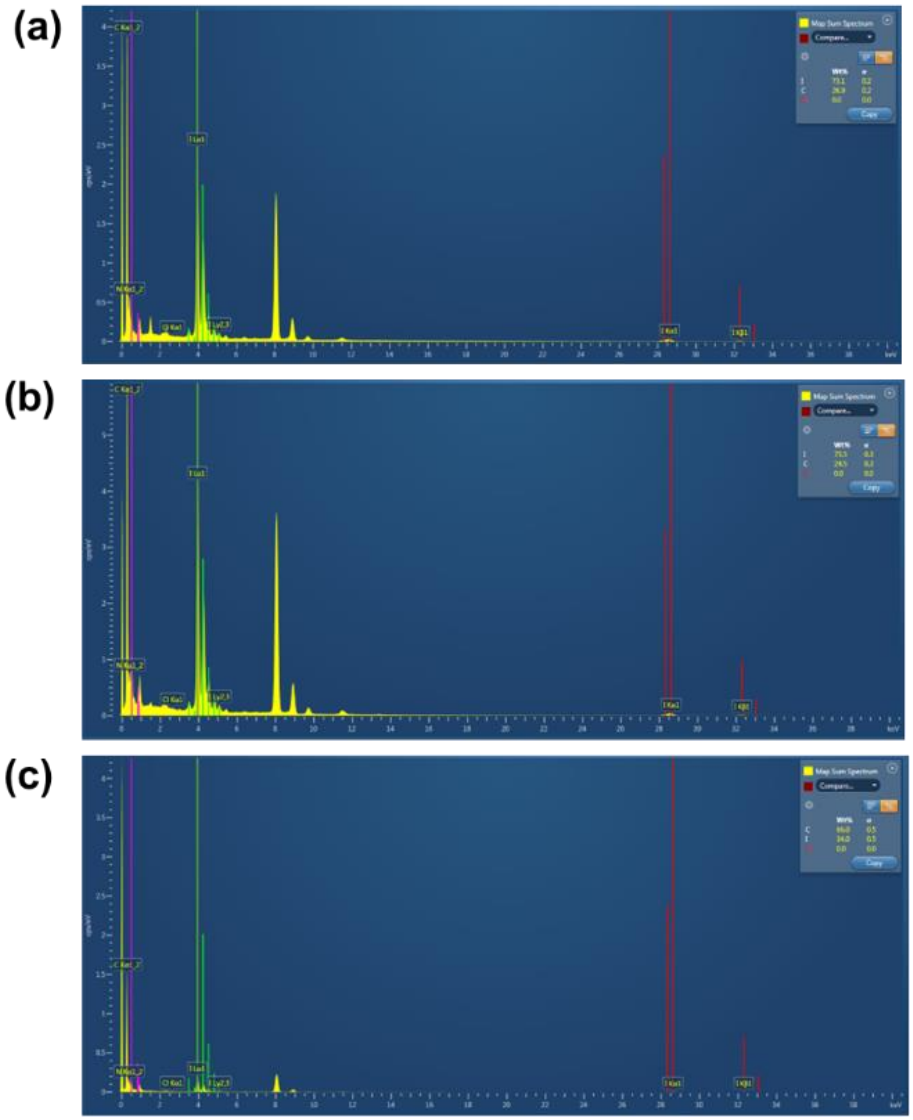

Figure 5.15: Energy-dispersive X-ray spectroscopy (EDS) data from HR-TEM experiment of (a) CH_3I@IP-VOF 1, (b) CH_3I@IP-VOF 2, (c) CH_3I@IP-VOF 3.

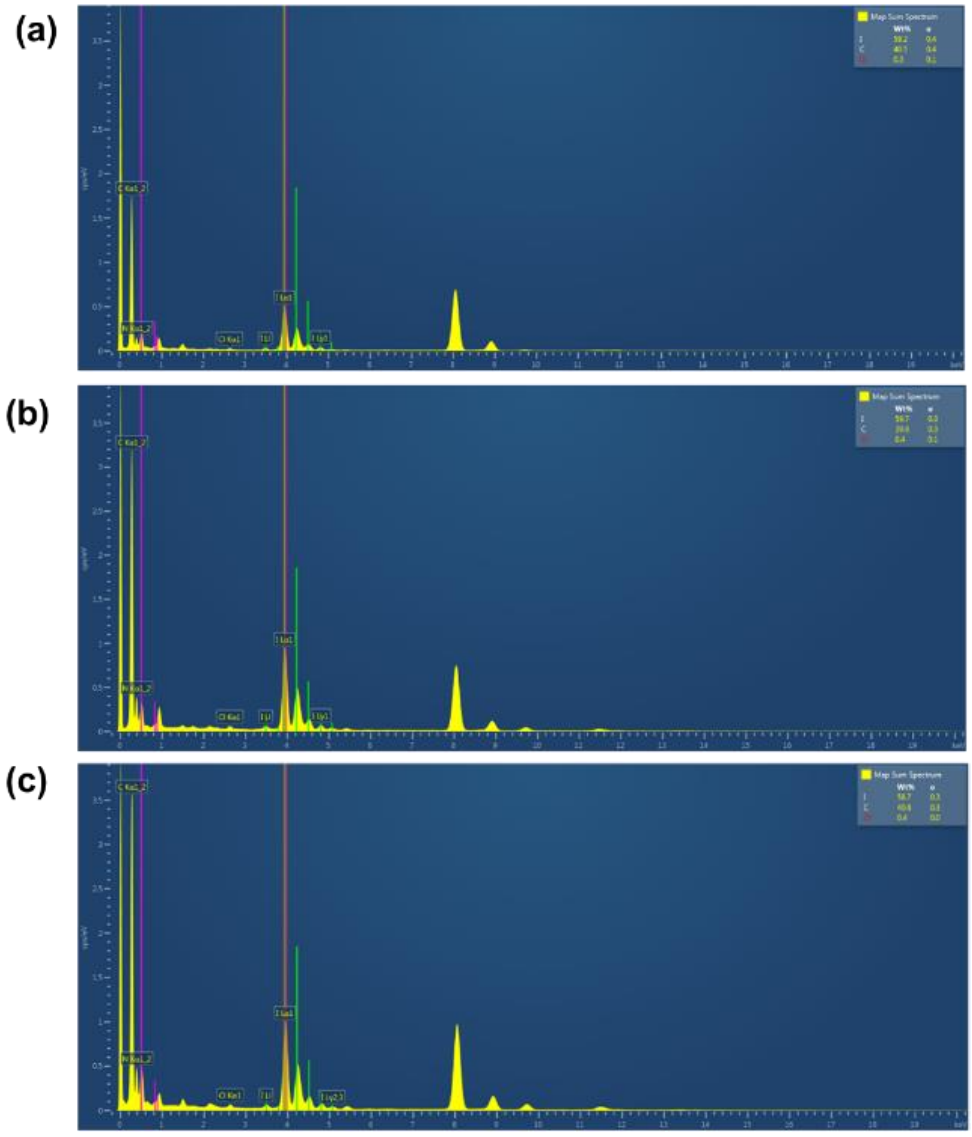

Figure 5.16: Energy-dispersive X-ray spectroscopy (EDS) data from HR-TEM experiment of (a) I_2@IP-VOF 1, (b) I_2@IP-VOF 2, (c) I_2@IP-VOF 3.

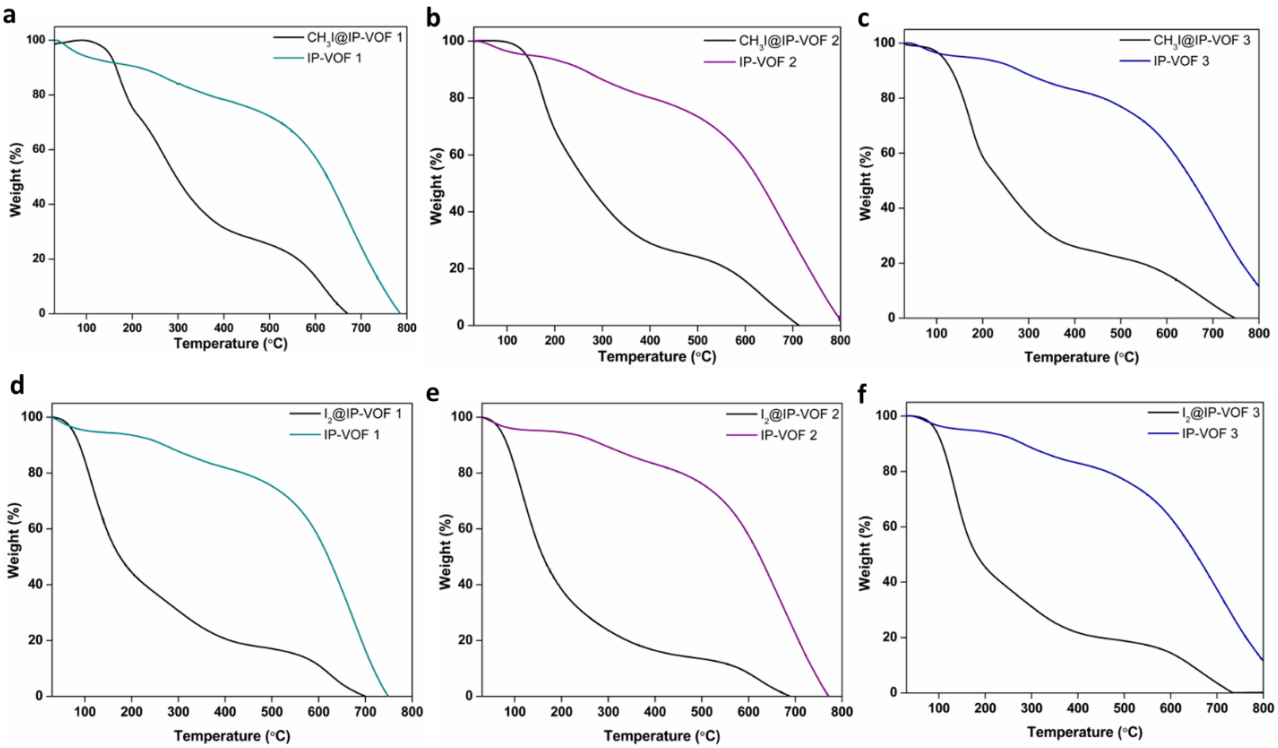

Figure 5.17: Thermogravimetric Analysis of (a) CH_3I@IP-VOF 1, (b) CH_3I@IP-VOF 2, (c) CH_3I@IP-VOF 3, (d) I_2@IP-VOF 1, (e) I_2@IP-VOF 2, and (f) I_2@IP-VOF 3

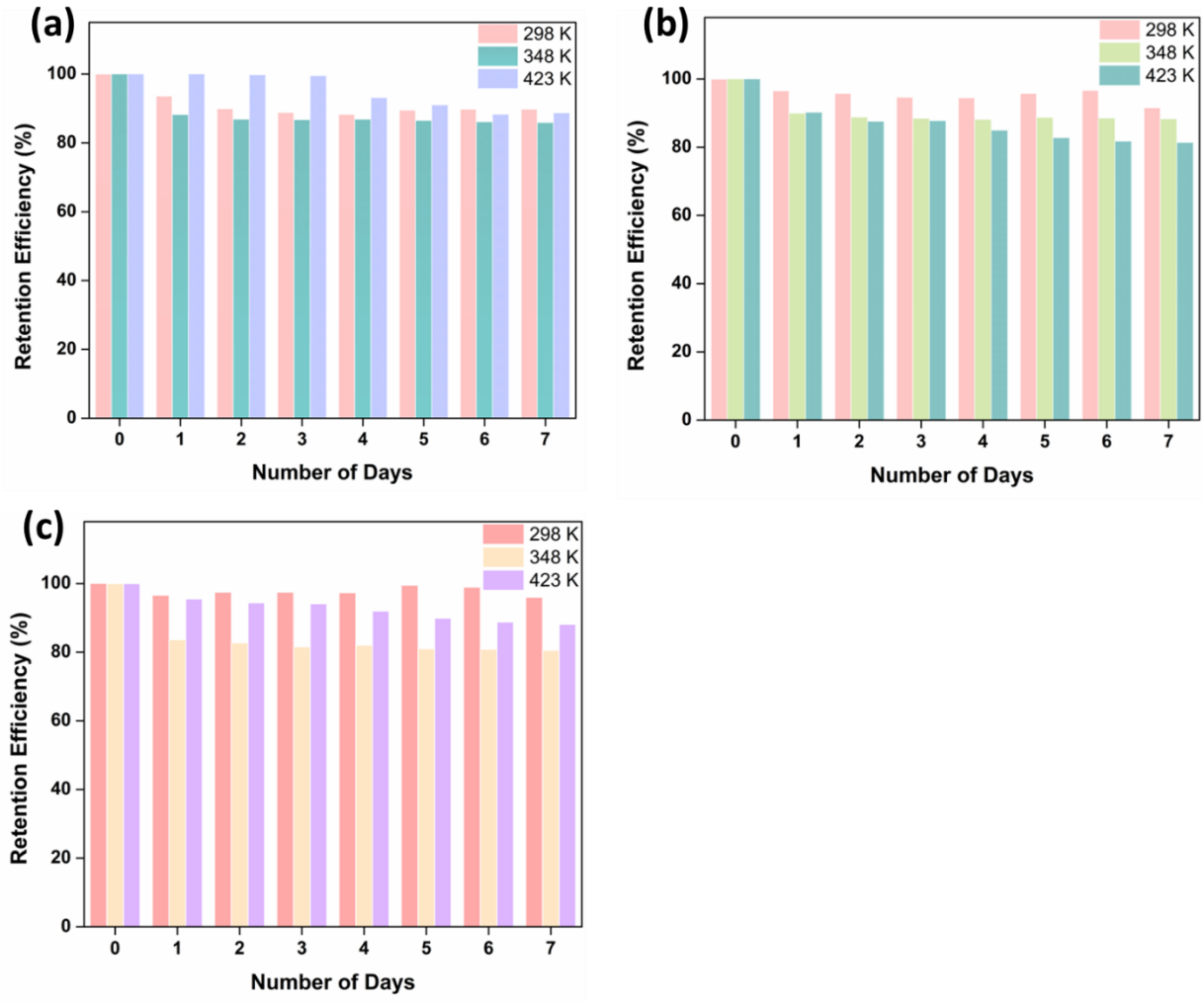

Figure 5.18: Methyl Iodide Retention Efficiency of (a) CH_3I@IP-VOF 1, (b) CH_3I@IP-VOF 2, and (c) CH_3I@IP-VOF 3 for 7 days at 298 K, 348 K, and 423 K

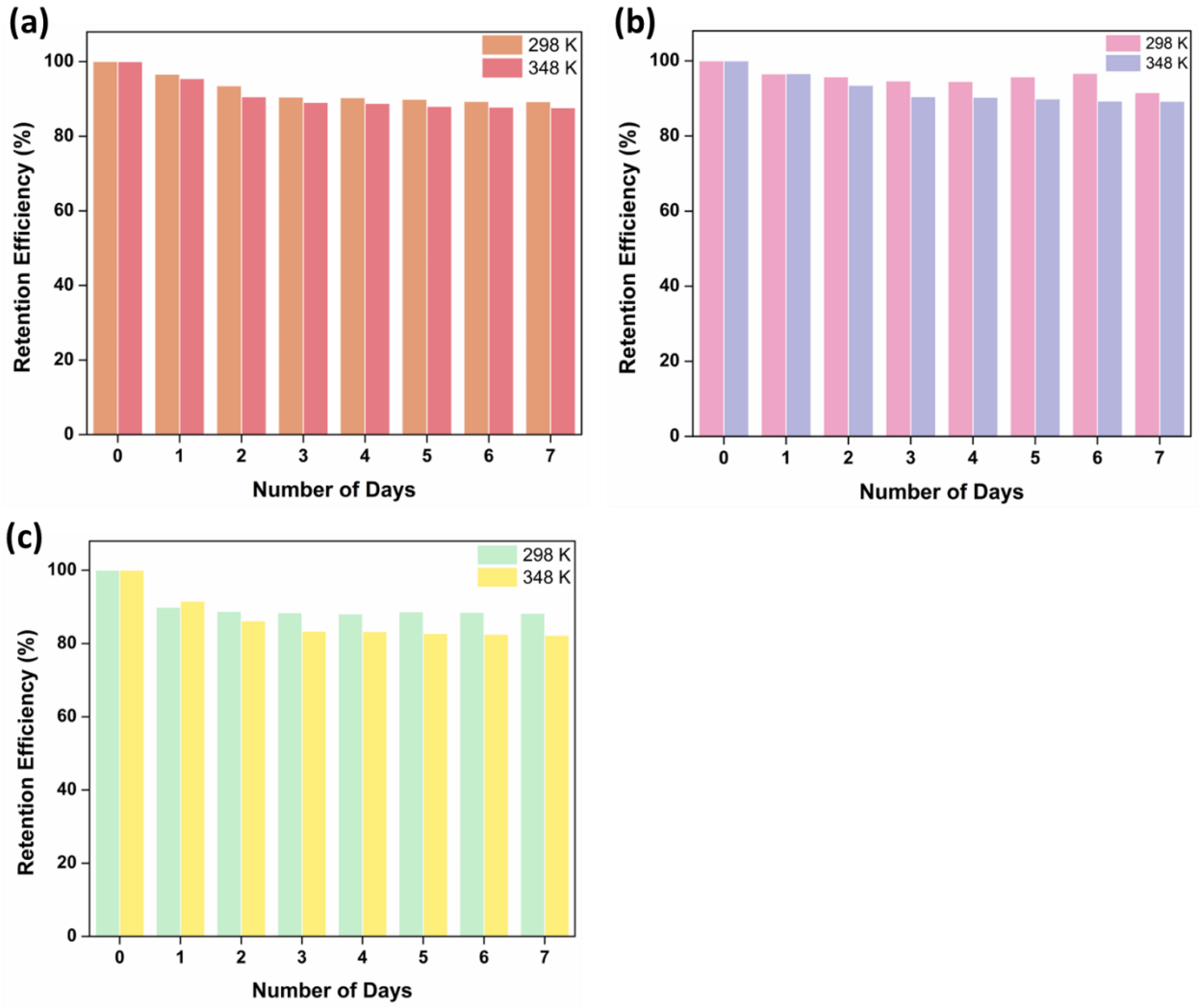

Figure 5.19: Iodine Retention Efficiency of (a) I_2@IP-VOF 1, (b) I_2@IP-VOF 2, and (c) I_2@IP-VOF 3 for 7 days at 298 K, 348 K, and 423 K

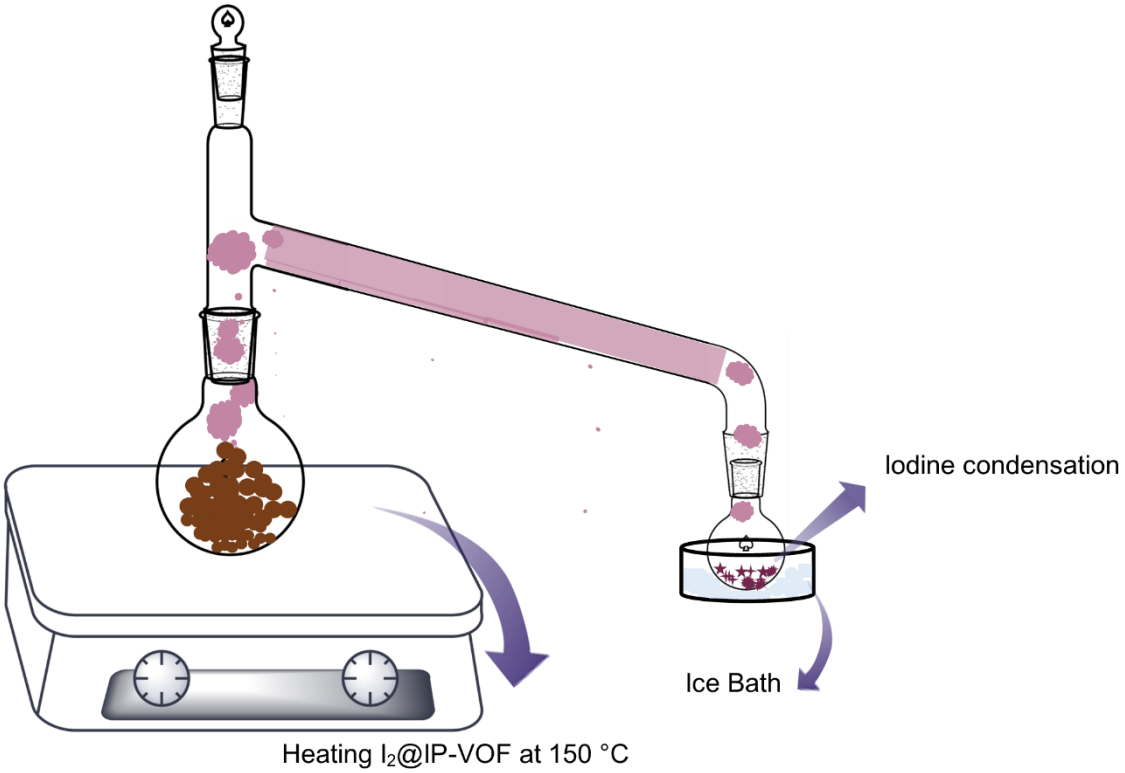

Figure 5.20: Schematic diagram of the experimental setup for Iodine Recovery.

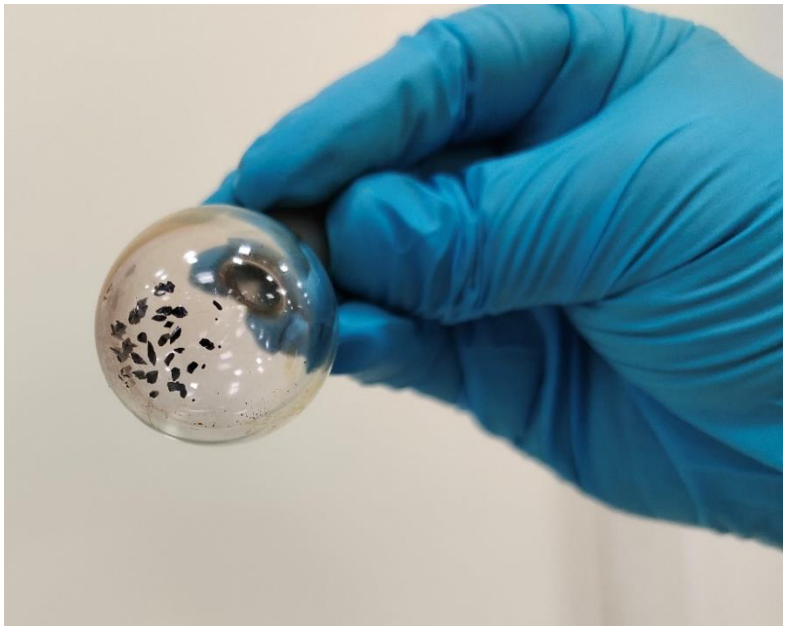

Figure 5.21: Digital image of recovered solid molecular Iodine.

References:

1. Davis, M. E. (2002). Ordered porous materials for emerging applications. *Nature*, *417*(6891), 813-821.
2. Bennett, T. D., Coudert, F., James, S. L., & Cooper, A. I. (2021). The changing state of porous materials, *Nature Materials*, *20*(**9**), 1179-1187.
3. J. Huve , A. Ryzhikov, H. Nouali, V. Lallia, G. Augé and T. J. Daou, Porous sorbents for the capture of radioactive iodine compounds: a review, *RSC Adv.*, 2018, **8**, 29248.
4. González-García, C., González, J., & Román, S. (2011). Removal efficiency of radioactive methyl iodide on TEDA-impregnated activated carbons. *Fuel Processing Technology*, *92*(**2**), 247-252.
5. Fajal, S., Mandal, W., Torris, A., Ultralight crystalline hybrid composite material for highly efficient sequestration of radioiodine. *Nat Commun* **15**, 1278 (2024).
6. S. Fajal, D. Majumder, W. Mandal, S. Let, G. K. Dam, M. M. Shirolkar and S. K. Ghosh, Unraveling mechanistic insights into covalent organic frameworks for highly efficient sequestration of organic iodides from simulated nuclear waste. J. Mater. Chem. A, 2023, **11**, 26580-26591
7. Xie, Y., Pan, T., Lei, Q., Efficient and simultaneous capture of iodine and methyl iodide achieved by a covalent organic framework. *Nat Commun* **13**, 2878 (2022).
8. Li, B., Dong, X., Wang, H. Capture of organic iodides from nuclear waste by metal-organic framework-based molecular traps. *Nat Commun* **8**, 485 (2017).
9. S. Asaftei, D. Huskens and D. Schols, HIV-1 X4 Activities of polycationic "Viologen" based dendrimer by interaction with the chemokine receptor CXCR4: Study of Structure Relationship. *J. Med. Chem*., 2012, **55**, 10405–10413.
10. P. Samanta, P. Chandra, S. Dutta, A. Desai and S. K. Ghosh, Chemically stable ionic viologen-organic network: an efficient scavenger of toxic oxo-anions from water. *Chem. Sci.*, 2018, **9**, 7874 —7881
11. Das, G.; Skorjanc, T.; Sharma, S. K.; Gandara, F.; Lusi, M.; Shankar Rao, D. S.; Vimala, S.; Krishna Prasad, S.; Raya, J.; Han, D. S.; Jagannathan, R.; Olsen, J. C.; Trabolsi., Viologen-Based Conjugated Covalent Organic Networks via Zincke Reaction. *J. Am. Chem. Soc.* 2017, ***139***, 9558– 9565

12. L. He, L. Chen, X. Dong, S. Zhang, M. Zhang, X. Dai, X. Liu, P. Lin, K. Li, C. Chen, T. Pan, F. Ma, J. Chen, M. Yuan, Y. Zhang, L. Chen, R. Zhou, Y. Han, Z. Chai and S. Wang, A nitrogen-rich covalent organic framework for simultaneous dynamic capture of iodine and methyl iodide. Chem 2021, **7**, 699–714.
13. T. Pan, K. Yang, X. Dong and Y. Han, Adsorption-based capture of iodine and organic iodides: status and challenges. J. Mater. Chem., 2023, **11**, 5460–5475.
14. K. Funabashi, T. Fukasawa & M. Kikuchi (1995) Investigation of Silver-Impregnated Alumina for Removal of Radioactive Methyl Iodide. Nuclear Technology, 109:**3**, 366-372.
15. S. Saurabh, S. Mollick, Y.D. More, A. Banerjee, S. Fajal, N. Kumar, M. M. Shirolkar, S.B. Ogale, and S.K. Ghosh, Covalent Organic Framework Featuring High Iodine Uptake for Li-Ion Battery: Unlocking the Potential of Hazardous Waste, *ACS Materials Letters* 2023 *5* (**9**), 2422-2430
16. H.P. Zhang, L.L. Gong, M.J. Yin, X.H. Xiong, Q.Y. Zhang, X.F. Feng, F. Luo, J.B. Carn ey, Y. Yue, Efficient organic iodide capture by a mesoporous bimetallic-organic framework, Cell Rep. Phys. Sci., **3** (2022)
17. Pan, T., Yang, K., Dong, X., Zuo, S., Chen, C., Li, G., Emwas, A., Zhang, H., & Han, Y. (2024). Strategies for high-temperature methyl iodide capture in azolate-based metal-organic frameworks. *Nature Communications*, *15*(**1**), 1-10.
18. Pham, T. C. T. et al. Capture of iodine and organic iodides using silica zeolites and the semiconductor behaviour of iodine in a silica zeolite. Energ. Environ. Sci. **9**, 1050–1062 (2016).
19. Chapman, K. W.; Chupas, P. J.; Nenoff, T. M. Radioactive iodine capture in silver-containing mordenites through nanoscale silver iodide formation. *J. Am. Chem. Soc.* 2010, ***132***, 8897– 8899.
20. Zhang, Z.; Dong, X.; Yin, J.; Li, Z. G.; Li, X.; Zhang, D.; Pan, T.; Lei, Q.; Liu, X.; Xie, Y.; Shui, F.; Li, J.; Yi, M.; Yuan, J.; You, Z.; Zhang, L.; Chang, J.; Zhang, H.; Li, W.; Fang, Q.; Li, B.; Bu, X. H.; Han, Y. Chemically stable guanidinium covalent organic framework for the efficient capture of low-concentration iodine at high temperatures. *J. Am. Chem. Soc.* **2022**, *144*, 6821– 6829.

21. Yan, Z., Yuan, Y., Tian, Y., Zhang, D., & Zhu, G. (2015). Highly Efficient Enrichment of Volatile Iodine by Charged Porous Aromatic Frameworks with Three Sorption Sites. *Angewandte Chemie*, *127*(**43**), 12924-12928.
22. Azambre, B., Chebbi, M., & Hijazi, A. (2019). Effects of the cation and Si/Al ratio on CH3I adsorption by faujasite zeolites. *Chemical Engineering Journal*, ***379***, 122308.
23. Vienna, J. D. (2010). Nuclear Waste Vitrification in the United States: Recent Developments and Future Options. *International Journal of Applied Glass Science*, *1*(**3**), 309-321.
24. D. R. Haefner and T. J. Tranter, Methods of gas phase capture of iodine from fuel reprocessing off-gas: a literature survey, INL/EXT-07-12299, Idaho National Laboratory, Idaho Falls, ID, 2007.
25. S. H. Bruffey, R. T. Jubin, J. A. Quantify the Extent of Physisorption on Silver Based Sorbents under VOG Conditions, Report No. FCRD-MRWFD-2016- 000357; ORNL/TM-2016/568 (2016).